ORIGINAL ARTICLE

Synergistic effects of boiler ash and polypropylene fibers on the mechanical and durability properties of fly ash-based geopolymer foam concrete

İhsan Türkel · Mehmet Uğur Yılmazoğlu · Mehmet Akif Alman · Ahmet Benli · Oğuzhan Yavuz Bayraktar · Gökhan Kaplan

Received: 11 January 2025 / Revised: 28 October 2025 / Accepted: 6 November 2025 / Published online: 19 November 2025

Abstract

This study investigates the mechanical, thermal, and durability performance of one-part geopolymer foam concrete (GFC) incorporating boiler ash (BA) as a partial replacement for fly ash (FA) and polypropylene fibers (PPF). Nine distinct mixtures were prepared with varying BA replacement levels (0%, 10%, and 20%) and PPF contents (0%, 0.5%, and 1%). Comprehensive testing was conducted to evaluate compressive and flexural strength, thermal conductivity, porosity, water absorption, sorptivity, freeze-thaw resistance, and high-temperature durability. The experimental results indicate that replacing FA with BA enhances the geopolymer matrix's mechanical and durability properties through improved gel formation and matrix densification. The optimal mixture, containing 20% BA and 0.5% PPF, achieved a 41.52% increase in compressive strength compared to the reference mixture (0% BA, 0% PPF). This mixture also exhibited the lowest porosity (23.82%), water absorption (16.76%), and sorptivity (8.28%), along with the highest thermal conductivity (0.619 W/mK). However, mixtures with higher BA and PPF contents experienced reduced high-temperature resistance, with strength losses of 16.2% and 27.1% observed at 400 °C and 900 °C, respectively. Durability assessments revealed significant improvements in freeze-thaw performance. The optimized mixture demonstrated minimal weight loss and significant compressive strength gains after 15 freeze-thaw cycles. Microstructural analysis confirmed the synergistic effects of BA and PPF in enhancing the matrix's densification, reducing pore connectivity, and bridging micro cracks. Additionally, BA's high calcium content contributed to the formation of dense C-S-H and C-A-S-H gels, which played a crucial role in enhancing strength and reducing permeability. This study underscores the potential of BA as a sustainable alternative to FA in GFC production, highlighting its role in waste valorization and environmental sustainability. The findings provide valuable insights for optimizing BA and PPF content in GFC formulations, promoting their application in eco-friendly and high-performance construction materials.

Keywords Environmental sustainability · Fly ash geopolymer foam concrete · Boiler ash · Durability · Strength · Thermal properties

1 Introduction

While developing energy-efficient buildings through research into various passive insulation technologies has become an important theme in construction, foam concrete (FC) qualifies as one of the best options due to targeted excellent thermal insulation [1]. The densities of foam concrete range from 200 to about 1600 kg/m³ [2] and are classified as cellular concrete made by air bubbling using a foaming agent [3]. It is innovation and good building material; foam concrete use is greatly increasing in these years, especially those in European and Asian countries [4]. Its distinct attributes-low self-weight [5], cost-effectiveness [6], workability enhancement [7], sound insulation [8], fire resistance [9], and low thermal conductivity [10] -are a very good fit for partition walls, backfills, backfilling construction projects, and non-load-bearing structures, as opposed to traditional concrete [11]. Indeed, the construction sector has been urged by the world to become more eco-friendly and sustainable because construction is known for its contribution to carbon emission and natural resource-use-at a very high scale [12]. Today, about 8% of global CO_2 emissions are produced by ordinary Portland cement (OPC)-based production of conventional concrete, the traditional precursor to FC [13]. In addition to this demand-and resource exhaustively, OPC-based concrete production causes extensive air pollution and ecological destruction, both of which caused through extensive sand and gravel mining [14]. Therefore, there is a growing interest in finding alternative cementitious materials for minimizing construction costs to environmental damage [15].

Such developments have resulted in the emergence of entirely new families of materials such as geopolymers and alkali-activated materials (AAMs) [16], which might offer 80% reductions in CO_2 emissions when compared with OPC [17]. AAMs would further leverage the utilization of waste products such as ground granulated blast-furnace slag (GBFS) [18], fly ash (FA) [19], and waste glass [20], significantly contributing to waste management [21]. Furthermore, AAMs have lower water demand as they require less water for their reaction compared with ordinary OPC [22]. They offer other advantages: rapid hardening [23], high early strength [24], and corrosion resistance [25], freezing [26], and fire [26]. The accumulative advantages hence lead to the extensive use of AAMs, wherein geopolymer foam concrete (GFC) is most studied due to its lightweight [27] and superior thermal insulating properties [28] that make it a suitable candidate for sustainable construction and energy-efficient building design applications [25], From the perspective of research, there has been significant progress in GFC during the last decade [29].

The inexpensive and resource-efficient production capacity of GFC is consistent with the growing trend adopting sustainability within the construction sector for the future. Nevertheless, GFC produced these days from by-products such as silica sand and GBFS - both of which can be considered useful industrial byproducts-are finite resources, use of which for production can have environmental ramifications, such as possible ecosystem disruption during sand extraction [4].The application of industrial and agricultural wastes as substitutes for virgin raw materials in GFC has been gaining special attention over the last decade [30]. Fly ash (FA), a byproduct of coal combustion, has been utilized in various concrete materials owing to its high pozzolanic reactivity and ability to enhance mechanical properties of GFC when blended with GBFS [31]. FA, another useful sustainable concrete ingredient can improve compressive strength and thermal performance when partially replacing GBFS [32]. In some cases, the durability and waterproofness of GFC may be compromised because large contents of FA can create more porous but less reactive material than GBFS [33]. While GFC has demonstrated notable advantages in energy efficiency and environmental sustainability, the material's performance still depends heavily on the choice and proportion of raw materials. FA has long been used in GFC due to its pozzolanic properties, which contribute to the strength and durability of the concrete [34]. Alkali-activated FA, while widely regarded as an optimal precursor for geopolymer production due to its abundant aluminosilicate content [35], is hindered by limitations such as low early strength development and slow setting rates [36]. These drawbacks primarily stem from the crystalline nature of a significant portion of the Si-Al phases in FA, which resist rapid dissolution in alkaline solutions. Consequently, during the initial stages of the geopolymerization process, only a minimal fraction of the FA undergoes activation, resulting in limited formation of reaction products essential for early

strength gain and rapid matrix consolidation. In addition, challenges associated with the availability, consistency, and quality of FA have prompted research into other industrial by-products. Recent studies highlight that valorizing industrial by-products can yield concretes that are both eco-efficient and structurally reliable. For instance, Das et al. [37] showed that using ferrochrome slag (FCS) and FA significantly reduced life cycle impacts while maintaining strength. Further, investigations on reinforced beams confirmed that FA-FCS concretes exhibited enhanced ductility, toughness [38], and shear performance compared to natural aggregate concrete, validating their safe structural application [39].

One such alternative is boiler ash (BA), a by-product of solid fuel combustion in industrial boilers. BA contains a high concentration of calcium oxide (CaO), which can contribute to the formation of calcium silicate hydrate (C-S-H) gels-key components for improving the mechanical strength and durability of geopolymer-based materials. Despite its potential, the use of BA in GFC has been relatively underexplored compared to FA, and its effects on the overall properties of the material require further investigation. In this study, BA used was specifically collected from coal-fired industrial boilers, and is therefore equivalent to bottom coal ash (BCA). Recent studies have shown the potential of BCA in geopolymer foam concrete (GFC), where it improves sustainability by valorizing industrial by-products. Soe et al. [40] reported that BCA-based porous geopolymers achieved compressive strengths of 0.75–6.86 MPa and low thermal conductivity (~ 0.32 W/m·K), making them suitable for thermal insulation. Similarly, Hosseini et al. [41] demonstrated that mechanochemical activation of BCA with FA enhances geopolymerization and improves strength, confirming BCA as a promising precursor in GFC systems. Incorporation of BCA into cellular lightweight geopolymer mortars has been shown to reduce both unit weight and thermal conductivity, with performance strongly influenced by foam dosage and mixture proportions [42]. Fine-ground BCA geopolymers have reported thermal conductivity values as low as 0.46 W/mK, significantly lower than OPC [43]. Furthermore, blending BCA with rice hull ash yields geopolymer concretes with reduced thermal conductivity (~ 0.578 W/mK) and enhanced heat resistance, while foamed geopolymers containing coal FA, BCA, and rice hull ash achieve ultra-low values (0.033–0.037 W/mK) compared to unfoamed samples (0.48 W/mK) [44]. These studies confirm the potential of BCA-based geopolymers as sustainable, low-heat-transmission, and fire-resistant construction materials.

In addition to binder materials, fibers such as polypropylene fibers (PPF) have been incorporated into cementitious mixtures to enhance mechanical properties, particularly in improving crack resistance and tensile strength [45]. The inclusion of PPF helps bridge micro-cracks and prevents their propagation under stress, thus improving the structural integrity and durability of the concrete [46]. While previous studies have demonstrated the positive effects of PPF on the performance of traditional concrete and geopolymer concrete [47], limited research has focused on its synergistic effects with BA in geopolymer foam concrete, particularly in terms of high-temperature resistance, freeze-thaw stability, and overall durability. The combined effects of BA and PPF on the mechanical, thermal, and durability properties of GFC have not been systematically studied. As the construction industry continues to seek materials that not only reduce environmental impact but also perform well under challenging conditions, it is essential to understand how alternative materials like BA and reinforcement technologies like PPF can be optimized in GFC formulations. This research aims to fill this gap by exploring the effects of BA as a partial replacement for FA and the influence of PPF on the mechanical, thermal, and durability properties of GFC. The study will investigate the optimal proportions of BA and PPF to enhance the performance of GFC in terms of compressive strength, flexural strength, thermal conductivity, porosity, water absorption, shrinkage, freeze-thaw resistance, and high-temperature stability. By addressing these key performance metrics, this research aims to contribute to the development of more sustainable, durable, and high-performance construction materials. The results of this study could offer valuable insights for the future use of BA and PPF in geopolymer-based foamed concrete, furthering the adoption of eco-friendly and resilient building materials in the construction industry.

1.1 Research gap

GFC has gained significant attention as a sustainable construction material due to its lightweight, thermal insulation properties, and reduced carbon footprint. While extensive research has focused on the use of industrial by-products such as FA and GBFS in GFC, limited studies have explored the incorporation of alternative waste materials like BA. BA, with its high calcium oxide content, has the potential to enhance binding phases such as calcium silicate hydrate (C-S-H) and improve the mechanical and thermal properties of GFC. However, its impact on durability, particularly under extreme environmental conditions such as high temperatures and freeze-thaw cycles, remains underexplored. Furthermore, although PPF are known to improve the mechanical properties and durability of cementitious materials, their synergy with BA in GFC matrices has not been fully investigated. The combined effects of BA and PPF on properties such as porosity, water absorption, shrinkage, and high-temperature resistance have not been systematically studied. This research addresses these gaps by evaluating the effects of BA and PPF on the mechanical, thermal, and durability properties of GFC. It provides insights into the optimization of BA and PPF content to achieve a balance between strength, durability, and thermal performance, thereby contributing to the development of eco-efficient GFC formulations for sustainable construction.

1.2 Research significance

The construction industry is under increasing pressure to adopt sustainable practices to reduce its environmental footprint and resource consumption. OPC, a primary binder in conventional concrete, is responsible for approximately 8% of global carbon dioxide emissions. GFC offers a promising alternative by utilizing industrial by-products as binders, reducing greenhouse gas emissions and promoting waste valorization. This research is significant as it explores the underutilized potential of BA, a by-product of solid fuel combustion, as a sustainable partial replacement for FA in GFC. Incorporating BA not only reduces dependency on conventional materials but also addresses waste management challenges by repurposing BA, which is often landfilled. The study also integrates PPF, which enhance the mechanical properties and durability of GFC, thereby extending its applicability in demanding environments. By investigating the combined effects of BA and PPF on the strength, durability, thermal insulation, and high-temperature resistance of GFC, this research provides valuable insights for the optimization of GFC formulations. It addresses critical issues such as shrinkage, porosity, and resistance to freeze-thaw cycles and high-temperature exposure, making GFC more viable for a wide range of construction applications. The findings contribute to advancing eco-efficient construction materials, aligning with global efforts to achieve sustainability goals. This research not only demonstrates a pathway to reduce carbon emissions and material waste but also opens new possibilities for creating high-performance, durable, and thermally efficient building materials, paving the way for a more sustainable construction industry.

2 Materials and methods

2.1 Materials

F-class fly ash (FA) conforming to ASTM C618 standard was used to prepare foam concretes produced in this study. The specific gravity of FA is 2.24, and the Blaine specific surface area is 2800 cm^2/g. In addition, ashes from solid fuel boilers used to obtain heat energy were used instead of FA in the mixtures. These boiler ashes (BA) were first reduced to fine aggregate size with the help of a crusher in the laboratory. Afterward, it was ground in a ball mill for 75 min and reduced to 125 μm. Since BA is obtained at lower temperatures than FA, the loss on ignition (LOI) is relatively higher. The boiler ash (BA) used in this study was sourced from a coal-fired industrial boiler and exhibits characteristics comparable to bottom coal ash, including its morphology and CaO content. Throughout this manuscript, BA is synonymous with bottom coal ash. The

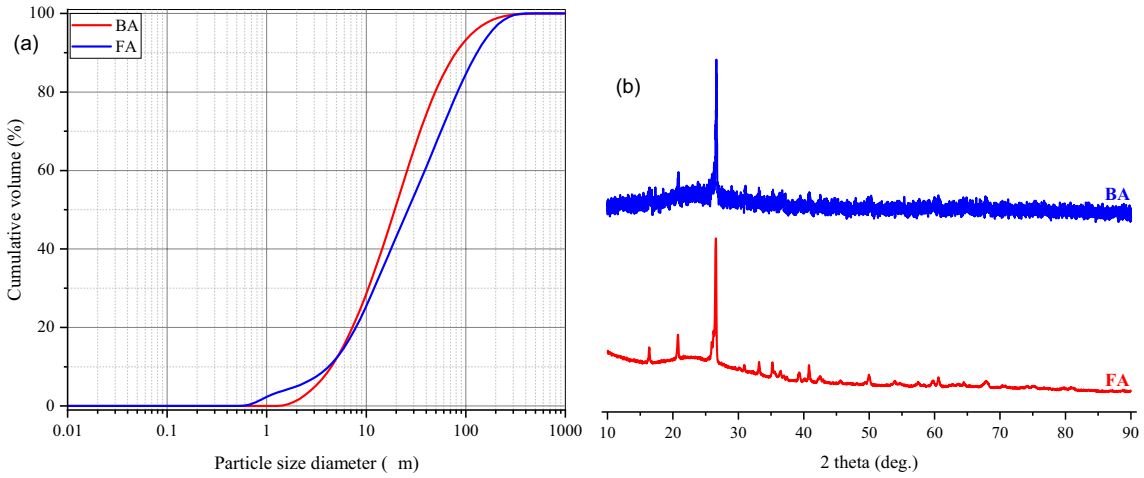

Fig. 1 Characteristics of FA and BA **a** size distribution **b** XRD pattern

Table 1 Chemical properties of FA and BA (% wt)

Oxide	CaO	SiO_2	Al_2O_3	Fe_2O_3	Na_2O	K_2O	MgO	SO_3	LOI
FA	3.7	56.7	25.9	7.3	0.6	1.7	1.1	0.3	2.5
BA	26.9	31.1	13.5	11.7	0.7	0.9	3.5	2.5	8.7

specific gravity of BA is 2.19, and the Blaine specific surface area is 3200 cm^2/g. The particle size distribution and mineralogical properties of FA and BA are given in Fig. 1. Figure 1a shows that BA reaches its 50% cumulative volume at about 10 µm, while FA reaches the same volume at about 20 µm. The cumulative distribution of FA increases more slowly than that of BA, indicating that FA contains larger particles in a more homogeneous distribution [48]. However, FA (red curve) appears to reach 20% of its cumulative volume with smaller particles. This indicates that FA presents a finer-grained distribution. BA (black curve) reaches 20% of its volume with larger particles. The XRD pattern for BA shows a dominant amorphous structure. This is consistent with an amorphous pattern where the amplitudes are generally low and broad peaks are seen (Fig. 1b). A large and distinct peak is visible around 2θ = ~26–28°. This mainly indicates quartz (SiO_2) mineral. The presence of low density and broad peaks indicates that BA has a more amorphous or glassy structure. This suggests that BA may have low pozzolanic properties or be less reactive than other materials. The XRD pattern for FA shows more distinct and sharp peaks, indicating more crystalline structures. In FA, a distinct quartz peak is also seen around 2θ = ~26–28°. In addition, other peaks probably indicate phases such as mullite ($Al_6Si_2O_{13}$), one of the phases formed at high temperatures in fly ash. The sharp peaks indicating more crystalline structures of FA suggest a mixture of crystalline and amorphous structures. This may indicate that FA contains amorphous silica, which increases its pozzolanic activity. The XRF method determined the FA and BA chemical properties, which are presented in Table 1. The CaO content of BA is considerably higher than FA. Also, the SO_3 content of BA is higher than FA.

Pumice aggregate was preferred as lightweight aggregate in foam concrete production. The specific gravity of pumice aggregate was 1.88, and the 24-hour water absorption was 15.8%. The particle distribution of pumice aggregate according to ASTM C33 is given in Fig. 2. The sieve opening of the pumice aggregate is between 0 and 4 mm. Appearances of FA, BA and pumice aggregate used in foam concrete production are given in Figs. 3 and 4.

The foaming agent used was sodium lauryl sulfate (SLS). SLS was used at a level of 10% by water weight, and these two components were mixed with a high-speed mixer to achieve a foam density of approximately 120 g/l. Sodium metasilicate in powder form was used to activate FA and BA. Sodium metasilicate powder has a

https://doi.org/10.1007/s43452-025-01369-2

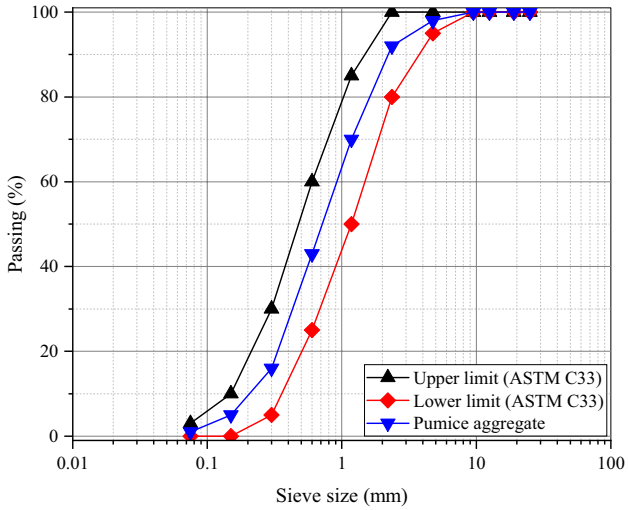

Fig. 2 Particle size distribution of pumice aggregate

Fig. 3 Appearance of FA, BA and pumice aggregate

Fig. 4 Flow diameters

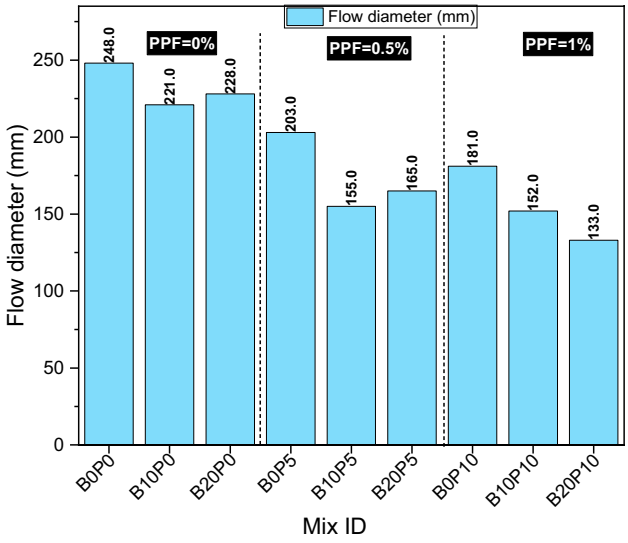

molecular weight of 122.06 g/mol. Its specific gravity is 2.61. Polypropylene fibers (PPF) of 6 mm length were also used to produce foam concretes. The technical properties of these fibers are presented in Table 2.

Table 2 Technical characteristics of PPF

Length (mm)	Diameter (μm)	Density (g/cm^3)	Tensile strength (MPa)	Young's modulus (MPa)	Elongation (%)
6	18	0.91	400	9000	40

Table 3 Mixing proportions and material quantities (kg/m^3)

Mix ID*	BA (%)	PPF (%)	FA	BA	PPF	Water	Foam	PA	Na_2SiO_3
B0P0	0	0	600	0	0.0	210	50	274	90
B10P0	10	0	540	60	0.0	210	50	291	90
B20P0	20	0	480	120	0.0	210	50	288	90
B0P5	0	0.5	600	0	4.6	210	50	284	90
B10P5	10	0.5	540	60	4.6	210	50	281	90
B20P5	20	0.5	480	120	4.6	210	50	279	90
B0P10	0	1.0	600	0	9.1	210	50	274	90
B10P10	10	1.0	540	60	9.1	210	50	272	90
B20P10	20	1.0	480	120	9.1	210	50	270	90

2.2 Mixing ratios, casting and curing processes of foam concretes

FA was preferred as the primary binder material in producing foam concretes. BA replaced FA in the ratio of 10 and 20 (by weight). PPF was added to the mixtures at 0.5 and 1.0% by volume. A total of 9 different mixtures were produced within the scope of the study. In producing all foam concretes, the water/binder ratio was 0.35, and the foam content was 50 kg/m^3. In addition, sodium metasilicate was added to the mixture at 15% by weight of FA and BA (if any). The mixture ratios of foam concrete and the weights of the materials used are given in Table 3.

In producing foam concretes, FA, BA, pumice and sodium metasilicate were mixed at 145 rpm for 1 min. Then water was added to the mixture, mixing at 145 rpm for 1 min and 280 rpm for 3 min. The mixture was mixed for one minute at 145 rpm then for two minutes at 280 rpm after the addition of foam in the third phase. PPF was then added to the mixture, and it was mixed for one minute at 145 rpm and three minutes at 280 rpm. After mixing, the specimens were placed in their molds. After the surface of the specimens was covered with stretch film, the thermal cure was started immediately. An oven with a heating rate of 5 °C was used for thermal curing. The samples were cured in an oven at 80 °C for 24 h [49]. The samples were allowed to cool in the oven. The samples were then removed from their molds and stored in laboratory conditions until the day of the experiment.

2.3 Test method

The flow diameter of the fresh samples was measured by placing them on a flow table by ASTM C1437 [50]. Physical properties such as water absorption and apparent porosity were determined according to the ASTM C642 [51] standard (50 × 50 × 50 mm specimens). Also, measurements were taken on the oven-dry density of these samples. Physical properties were evaluated after 28 days. The flexural and compressive strengths of the geopolymer foam specimens were measured at 7, 28 and 91 days. To determine mechanical performance, prism specimens measuring 40 × 40 × 160 mm were produced. The specimens were tested in three-point bending according to ASTM C348 [52]and then upon the compressive strength as per ASTM C349 [53]. The samples' mechanical characteristics and mass loss were assessed after exposure to 200, 400, and 900 °C. 40 × 40 × 160 mm prism specimens were made to evaluate their ability to withstand high temperatures. After being allowed to cure for 28 days, the samples were heated to high temperatures in a muffle furnace at 10 °C per minute.

The specimens were kept at the specified temperatures for two hours before being taken out of the furnace and given time to cool in a lab setting. Following that, the water absorption through the geopolymer foam samples' capillary channels was assessed using the TS EN 1015-18 [54]standard. Samples of 50 × 50 × 50 mm cubes were created explicitly for this purpose. The samples' sorptivity properties were determined after a 28-day curing

process. The samples underwent 15 and 30 cycles of freeze-thaw (F-T). The ASTM C666 [55]standard was used to quantify the specimens' weight loss and compressive strength. Prism specimens of 40 × 40 × 160 mm were subjected to F-T cycles. It takes seven hours to freeze at -20 °C and five hours to defrost at + 4 °C. 28-day samples were subjected to F-T cycles. The specimens' drying shrinkage behavior up to day 120 was also examined. To achieve this, mortar bars measuring 25 × 25 × 285 mm were produced by ASTM C596 [56] requirements. Following a 24-hour heat curing period, the specimens' original lengths were measured. After that, on days 7, 14, 21, 28, 56, and 90, the length changes of the specimens housed in the lab were measured using a digital comparator. Plate specimens measuring 500 × 500 × 30 mm were created to determine the specimens' thermal conductivity coefficients. Following a 28-day curing period, the specimens were dried for three days at 50 °C before their thermal conductivity coefficients were determined.

3 Results and discussion

3.1 Fresh properties

Figure 5a depicts the effect of substituting FA with BA at replacement levels of 0%, 10%, and 20%, combined with varying PPF contents of 0%, 0.5%, and 1%, on the flowability of GFC mixtures made entirely with PA.

The flow diameter values ranged from 133 mm to 248 mm, indicating significant variation in workability resulting from the replacement of FA with BA and the incorporation of PPF. To ensure consistency in the analysis, the alkaline solution-to-binder ratio and foaming agent content were kept constant across all mixtures. The largest flow diameters are found in the mixtures devoid of PPF; the reference mixture, which contains 100% FA, has the largest flow diameter, measuring about 248 mm. FA is a fine spherical material which serves as a lubricant in concrete mixtures. In the reference mixture with 100% FA, these particles improve the flowability by reducing the friction between aggregates, resulting in increased flowability [57]. This is especially shown in mixtures without other ingredients such as fibers which may interfere with this lubrication action [58].

A progressive drop in flow diameter is seen as the amount of FA replaced with BA rises, suggesting decreased workability. FA is characterized by having a generally spherical or rounded side, which allows the particles of FA to be more easily poured or poured without friction and aids in improving the workability of internal friction. In comparison, BA displays angular or irregular particles, which interlock with one another to create increased frictional resistance, thus hindering its free flow and decreasing the workability and flow diameter. This surface

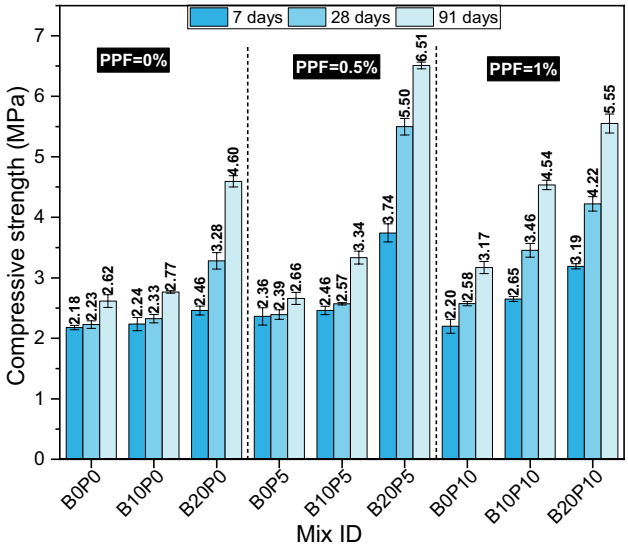

Fig. 5 Compressive strength during 7, 28, and 91 days of GFC combinations

area of BA is more compared to that of FA. In this context, more water would be needed when BA is substituted for FA to keep the consistency of the mixture, since the increase in the area of the particles of BA absorbs more water. Water is needed to coat the particles and ensure sufficient hydration; however, it reduces the free water available to keep the mix fluid. Thus, the mixture becomes sterner and less workable. The effect of adding BA with an increased content, therefore, caused a gradual lowering of flow diameter [59]. BA generally exhibits higher reactivity than FA in alkali-activated systems, largely due to its elevated calcium oxide content and irregular particle morphology [60]. The greater availability of reactive calcium species accelerates the precipitation of calcium silicate hydrate (C-S-H) and calcium aluminosilicate hydrate (C-(A)-S-H) gels, which not only contribute to enhanced mechanical strength but also result in a denser and more cohesive microstructure [61]. As BA content increases, this leads to greater gel formation that produces stiffer mixes, which resist flow. While the reaction tends to improve strength, it also decreases the fluidity and workability of the material, thus contributing towards further reduced flow diameters. More angular particles and more gel formation for increasing BA instead of FA lead to an increase in overall viscosity and cohesiveness of the mix [62]. This makes a mixture that is much more coherent, much thicker, and does not flow as easily as a mixture with higher FA content; it should be much more mobile and flowing. FA has a lower water absorption ratio than BA, requiring less water for hydration and enabling more free water in the mix for lubrication. Lubrication makes the mixture easier to spread, which improves flowability. In contrast, replacing FA with BA increases the water requirement while decreasing the amount of free water in the mix, affecting lubrication and subsequently flow diameter. The absence of sufficient lubrication creates higher resistance against flow, which reduces the flow diameter.

When 0.5% PPF is added to mixtures, the flow diameter decreases for all binder compositions. The flow diameter steadily decreases as the BA content rises, indicating that workability is adversely affected by both PPF inclusion and BA substitution. The mixtures with 1% PPF have the smallest flow diameters; the mixture with 20% BA has the lowest flow diameter, measuring 133 mm. Workability is significantly reduced when PPF content and BA replacement are high, most likely as a result of the fibers' effect on the cohesiveness and flow of the mixture [61]. When added to the mixture, PPF adds fiber reinforcement, which raises the mix's internal friction [33]. Because the fibers physically obstruct particle motion, thereby "bridging" the spaces between them, they increase flow resistance [63]. The combination thus becomes less fluid and more cohesive, which causes the flow diameter to drop. Additionally, PPF has a tendency to absorb water, which lowers the quantity of free water that may be used for lubrication. As a result, the mix becomes less workable and more viscous, which lowers the flow diameter. Fiber absorption causes the water content to decrease, which stiffens and makes spreading the mixture more difficult. As the fiber content rises, especially with 1% PPF, the fibrous network that forms inside the mix may further impede particle mobility, hence decreasing the mixture's workability and fluidity. The smallest flow diameters at 1% PPF are the outcome [47]. In comparison to FA particles, BA particles are typically angular and have a larger surface area. Internal friction between particles rises when BA takes the role of FA because the angular particles are more prone to interlock, which hinders movement and reduces workability. Because of its larger surface area and rougher texture, BA needs more water to maintain the same fluidity as FA. The extra water needed for hydration of BA actually binds the mix more strongly, reducing the available free water for lubrication, and making the mixture less fluid. This leads to a reduction in flow diameter as the BA content increases. Increased cohesiveness accompanying the substitution of BA in the mix and interaction between BA particles thus increases the viscosity of the mix. The increased viscosity hinders the flow of the mixture making it difficult to spread, thus leading to lower flow diameter. The inclusion of fibers (PPF) has a synergistic effect along with BA for the increase of cohesion and viscosity of the mix. While PPF adds to the internal friction and hinders flow [64], BA causes more interlocking of particles while itself needing more water, which makes the mixture stiffer and less fluid. Thus, the combination of higher PPF and substitution with BA further reduces free, available water through fiber absorption and more water demand placed by BA, which is highly restrictive in terms of the lubrication necessary to keep the mixture workable. All of this very much increases rigidity and reduces flowability, as shown by the low flow diameter.

3.2 Compressive strength

Figure 5a illustrates the influence of replacing FA with BA at substitution levels of 0%, 10%, and 20%, in conjunction with varying PPF contents of 0%, 0.5%, and 1%, on the mean compressive strength of GFC mixtures incorporating 100% PA.

The samples were subjected to initial curing at 80 °C for 24 h, followed by ambient curing for periods of 7, 28, and 91 days. The compressive strength of all GFC mixtures showed a progressive increase with extended curing durations, suggesting continued hydration reactions and potentially enhanced geopolymerization processes over time. The replacement of FA with BA enhanced the compressive strength of GFC mixtures, achieving the highest strength at a 20% BA content (20% BA and 80% FA), irrespective of the PPF content. BA has 26.9% CaO, which is much more than FA's 3.7% [65]. This increased calcium concentration promotes the formation of calcium silicate hydrate (C-S-H) gel [66], which is an important phase for strength development in geopolymer system [67]. The ideal BA level of 20% is anticipated to give enough CaO to build a dense and strong matrix while remaining in balance with the reactive aluminosilicates from FA. BA has a larger Blaine specific surface area (3200 cm^2/g) than FA (2800 cm^2/g), suggesting smaller particles and stronger reactivity. Furthermore, BA has a faster cumulative particle size distribution, which leads to improved particle packing, reduced porosity, and increased matrix densification, all of which contribute to higher compressive strength. At 20% replacement, BA may complement the spherical particle shape and aluminosilicate concentration of FA. This synergy enhances geopolymerization reactions and optimizes the microstructure, resulting in a balance that maximizes strength. Although BA has a higher loss on ignition (LOI) than FA (8.7% vs. 2.5%), its amorphous structure, as revealed by XRD research, contributes to reactivity. This reactivity promotes the formation of stronger geopolymeric linkages at the 20% BA replacement threshold. BA's high CaO and SiO_2 content (31.1%) promotes efficient gel formation and matrix densification [61, 68, 69]. The recommended replacement amount of 20% guarantees that the favorable benefits of BA are maximized while not weakening the overall binding strength.

The incorporation of PPF led to an enhancement in the compressive strength of the mixtures compared to those without PPF. Among the tested mixtures, the combination of 0.5% PPF and 20% BA replacement for FA resulted in the highest compressive strength. Furthermore, at 1% PPF, the mixtures with 0% and 10% BA exhibited the greatest compressive strength relative to the corresponding mixtures containing 0% and 0.5% PPF at the same BA substitution levels.

Under load, PPF bridges micro cracks in the matrix by acting as reinforcement [70]. This process delays failure and increases the material's capacity to withstand compressive loads by stopping the cracks from spreading. Stress concentrations near voids or microstructural flaws are lessened by the fibers' improved capacity to disperse applied stresses more uniformly throughout the matrix [71]. Better overall mechanical integrity results from this. By adding a ductile phase to the geopolymer matrix, PPF increases the material's resistance to abrupt brittle failure. Since of this, the material's compressive strength increases since it can undergo little deformation under stress without failing catastrophically. By interacting with the aggregates and binder, PPF strengthens the matrix's cohesiveness. This reduces the likelihood of internal weaknesses or segregation, resulting in a denser and more robust structure. PPF reduces the development of shrinkage cracks during curing by providing resistance to tensile stresses that arise as the matrix sets and hardens. The reduction in pre-existing micro cracks improves compressive strength. PPF distributes uniformly throughout the matrix at a dosage of 0.5% with little to no clustering or agglomeration. This guarantees that the fibers are fully incorporated into the matrix, optimizing their capacity for reinforcement and averting the development of weak spots [72]. The best compromise between matrix continuity and crack resistance is offered by the 0.5% PPF dose [73]. While lower fiber levels (e.g., 0%) might not provide adequate crack-bridging reinforcement. higher fiber contents (e.g., 1%) may result in fiber overcrowding, increasing porosity, and decreasing matrix compactness. The fibers efficiently bridge and arrest micro cracks that develop under stress at 0.5% PPF, lowering the chance of crack propagation [74]. By preserving structural integrity under compressive stresses, this process improves the material's overall strength and durability. By creating binding phases like C-S-H and C-A-S-H, boiler ash aids in the development of strength [75]. In

order to strengthen the matrix and prevent shrinkage-induced cracking, which could otherwise reduce strength, 0.5% PPF is added to the process. At 0.5% PPF, the fiber content is sufficient to significantly reinforce the matrix without introducing excessive voids or fiber clumping, which could reduce strength. This is why mixtures with 0.5% PPF and 20% BA achieve the highest compressive strength [76]. The combined use of 20% BA as a substitute for FA and 0.5% PPF resulted in the highest compressive strength among the tested mixtures, demonstrating a 41.52% improvement compared to the mixture containing 20% BA without PPF. This significant enhancement underscores the synergistic interaction between the partial replacement of FA with BA and the optimal reinforcement provided by 0.5% PPF, effectively contributing to the improved mechanical performance of the matrix [77].

Conversely, mixtures incorporating 1% PPF demonstrated superior performance when BA was used as a substitute for FA at replacement levels of 0% and 10%, particularly at the later curing age of 28 and 91 days. This suggests that higher fiber content effectively enhances the mechanical properties of the matrix in mixtures with 0 and 10% BA substitution levels. At 1% PPF, the fibers create a strong network inside the matrix that can stop cracks from spreading under stress and bridge micro cracks. This capability aids in the matrix's increased stress tolerance, especially as the material ages and the curing processes proceed. By enhancing the matrix's capacity to redistribute stressors, PPF lowers concentrations of localized stress. With higher fiber contents, this effect is especially advantageous since the fibers serve as reinforcements inside the geopolymer matrix, gradually increasing its mechanical strength. When FA is used alone, a matrix with a decreased calcium concentration, acceptable workability, and mild reactivity is produced. In this case, the 1% PPF addition strengthens the matrix and lessens the impacts of decreased gel formation, making up for FA's poorer mechanical performance. The development of C-S-H and C-A-S-H gels is improved when a tiny amount of FA is substituted with BA since this increases the amount of CaO in the system. These gels increase the density and strength of the matrix. This enhanced matrix further improves mechanical qualities by creating an ideal balance with the reinforcing impact of 1% PPF. Over time, both FA and BA support continuous hydration processes and geopolymerization. The matrix gets denser and more compact at later curing ages (28 and 91 days) as a result of the ongoing development of reaction products such C-S-H and C-A-S-H gels [78]. The fibers are more successfully incorporated in the geopolymer structure as the matrix densify with curing. This integration results in improved mechanical performance by strengthening the matrix's resistance to cracking and deformation under compressive pressures. A 10% substitution of BA adds enough calcium to encourage the development of strength without overburdening the matrix with unreacted particles. The fibers may operate at their best inside a robust and cohesive matrix thanks to this equilibrium. Combining BA and PPF reduces porosity because the fibers' ability to bridge cracks is enhanced by the dense matrix that BA creates, making the material stronger and more durable.

3.3 Flexural strength

Figure 6a presents the effect of replacing FA with BA at substitution levels of 0%, 10%, and 20%, combined with PPF contents of 0%, 0.5%, and 1%, on the mean flexural strength of GFC mixtures prepared with 100% PA. The mixes were first cured for 24 h at 80 °C, and then they were allowed to cure for 7, 28, and 91 days in the open air. With longer curing times, the results show a progressive increase in both flexural and compressive strengths, which is consistent with the ongoing evolution of hydration and geopolymerization reactions over time. In other words, as these chemical reactions progress, the material's strength keeps growing, improving the concrete's mechanical qualities. This suggests that the formation of binding phases, such as C-S-H and C-A-S-H gels, continues during prolonged curing, contributing to the development of a denser and more cohesive matrix.

Consistent with the compressive strength findings, the replacement of FA with BA enhanced the flexural strength of GFC mixtures, achieving the highest strength at a 20% BA substitution level (20% BA and 80% FA), irrespective of the PPF content. Compared to FA, BA typically has a higher calcium content along with higher reactivity. This thus results in the formation of additional binding phases such as C-S-H and C-A-S-H gels [78]. The bonding strength of the matrix increases because of formation of these phases, resulting in improved flexural properties. A 20% substitution of FA with BA has shown to yield optimal results in this regard. FA works

 https://doi.org/10.1007/s43452-025-01369-2

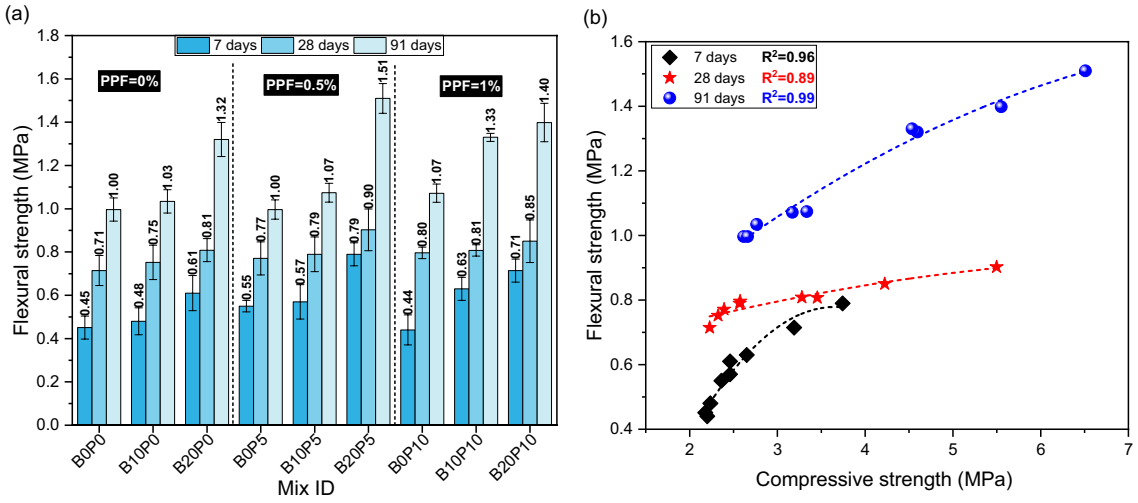

Fig. 6 Flexural strength values (**a**) and the relationship between flexural and compressive strength (**b**)

through the geopolymerization process whereby it gives the aluminosilicate precursors while BA enhances the availability of calcium for accelerated hydration and matrix densification [79]. The two thus result in a strong and cohesive microstructure and high flexural strength. In addition, incorporation of BA promotes denser geopolymer matrix with low porosity hence reducing the ability of material to bend stresses. This denser configuration rapidly distributes the loads applied and hence contributes greater performance in flexure as well. BA at a substitution level of 20% can provide the required reactive calcium without excessively diluting the aluminosilicate content from FA. Higher substitution levels (e.g., 30% or more) may reduce the aluminosilicate precursor availability, weakening the geopolymer network and diminishing the flexural strength. Thus, it is expected that not only matrix properties but also the bond between the matrix and PPF may increase due to substitution of BA. Thanks to this compatibility, PPF can better close cracks and distribute stresses, thus improving flexural strength [64]. The inclusion of PPF resulted in an enhancement of the flexural strength at all curing ages, with the highest flexural strength observed at 90 days in the mixture containing 0.5% PPF and 20% BA, representing the optimal performance among all the tested mixtures [80]. The geopolymer matrix has a reinforcing effect from PPF. It enables crack bridging due to stresses, preventing their propagation and improving the resistance to bending of the material [81]. This imparts improved flexural strength at the later curing stages (i.e., 28 and 91 days), when the matrix has attained higher strengths and could interact more appropriately with the fibers. 20% BA imparts greater reactivity as compared with FA, which enhances the process of geopolymerization and additionally aids in achieving a denser matrix. When combined with PPF, this densified matrix provides a better environment for the fibers to exert their reinforcement action, promotes more efficient stress distribution and ultimately improves flexural strength [82]. The 0.5% PPF level is the ideal point boosting flexural strength: it sufficiently boosts the matrix without greatly hindering the workability of the mixture. Excessive fiber entanglement may occur at a higher PPF content thereby affecting adversely the uniform distribution and overall performance [73]. The geopolymerization reactions continue to develop, resulting in greater densification and ultimate strength gain in the matrix over longer curing durations. 90 days of curing would allow the full realization of PPF reinforcement and BA substitution since the material would continue developing a stronger internal structure that was capable of transferring stresses more efficiently. The combination of BA's high reactivity and the PPF augments the bonding between the fibers and the geopolymer matrix, thus improving the load transfer between them. As the matrix becomes denser and more cohesive over time, the fibers' reinforcing capabilities are further optimized, particularly at the 90-day mark.

The relationship between compressive and flexural strength for GFC mixtures was studied up to 7, 28, and 91 days of curing, as shown in Fig. 6b. Relationship-wise, a strong positive association existed between compressive

and flexural strengths with correlation coefficients (R^2) being 0.96, 0.89, and 0.99 for compressive and flexural strengths at 7, 28, and 91 days, respectively. The high levels of correlation further indicate that the two properties are related to each other and that both properties will be increasingly developed with increased time under the geopolymer matrix. Here, it was observed that while there was a process of hydration and geopolymerization reactions, the outside and inside portions of the pure geopolymer matrix would also undergo densification, further contributing to an increased resistance value against both compressive and tensile stresses, hence linking compressive and flexural strength together [4].

3.4 Dry unit weight

Figure 7a presents the effect of replacing FA with BA at substitution levels of 0%, 10%, and 20%, combined with PPF contents of 0%, 0.5%, and 1%, on the mean dry unit weight of GFC mixtures prepared with 100% PA. The mixtures were subjected to an initial curing process at 80 °C for 24 h, followed by ambient curing for 28 days. The dry unit weight of the mixtures ranged from 1021 to 1788 kg/m³. The lowest dry unit weight was observed in the reference mixture containing 100% FA and 0%PPF. In contrast, the highest dry unit weight was achieved in the mixture with 20% BA (20% BA and 80% FA), corresponding to a 19.76% increase relative to the reference mixture. This mixture also demonstrated the highest compressive strength among all tested combinations due to the combined effects of matrix densification, enhanced reactivity from BA, optimized particle packing, and reduced porosity. These factors work together to create a robust and cohesive structure, making this mixture the most mechanically efficient and durable among the tested samples.

Compared to FA, BA typically has a finer particle size distribution and irregular, angular-shaped particles. These make the applications denser because of a tighter packing of particles in the matrix, which reduces void spaces and increases overall density. FA is comprised of more spherical particles which do prove beneficial in workability; however they are not that densely packed as angular BA particles are. Inadequately balanced by BA, the presence of larger or similar-sized FA particles leads to porosity again. BA and FA use together create a superior optimized particulate packing configuration because the angular BA particles interlock with spherical FA particles, thus minimizing the voids and creating a denser structure of matrix. This synergistic interaction enhances the dry unit weight by effectively utilizing the available space within the mixture. In general, BA has a considerably higher CaO level than FA's (26.9% vs. 3.7%). Higher CaO levels favor the formation of calcium silicate hydrate (C-S-H) and calcium aluminosilicate hydrate (C-A-S-H) gels in the course of geopolymerization, and both are important constituents for binding particles together to densify the matrix with an increased dry unit weight. The same was true on the contribution of FA to the geopolymer network based on the silica and

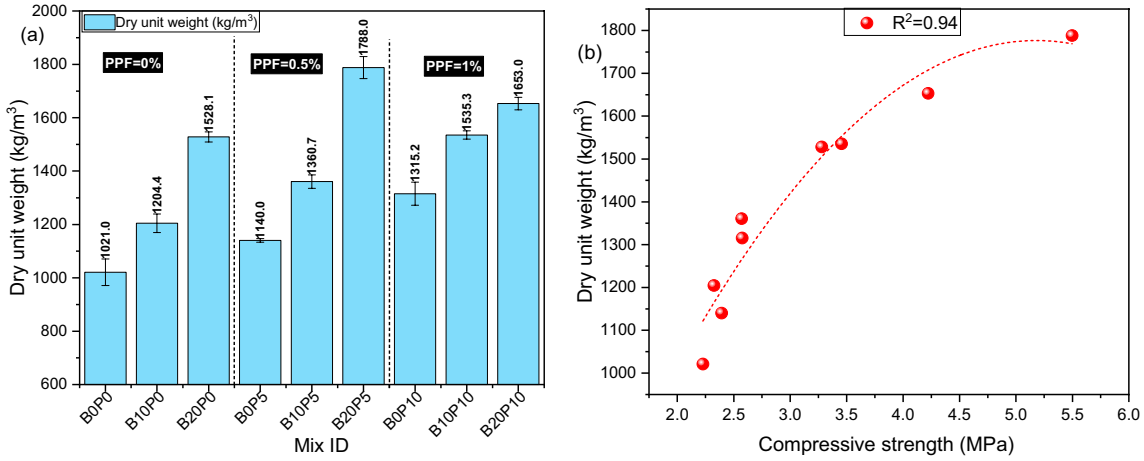

Fig. 7 The findings for oven dry density (**a**) and the relationship between dry density and compressive strength (**b**)

alumina, but from the lower CaO content, it follows that C-S-H and C-A-S-H gels formulated would also be lower when compared to these produced from BA, and with that, the densification of matrix may be also low. The higher reactivity of BA hastens geopolymerization reactions and accelerates the rapid formation of binding phases that densify the matrix. This reaction kinetics supports the result of a more tightly cohesive and bonded structure, thus increasing the dry unit weight. Thus, higher CaO contents with reactivity from BA make for a finer and denser microstructure. More additional binding gels fill and much better sealed pores, which contribute to reduced porosity and densification of the material. Improved bonding due to greater BA contents gives rise to a more homogeneous and less porous matrix. This not only raises the dry unit weight but also provides better mechanical properties such as compressive strength. Cure the sample under 80 °C for 24 h in the beginning to dissolve reactive species from BA and initiate the geopolymerization reaction. Following that, the sample is cured naturally to maintain the hydration and continued formation of gels that further densify the matrix. Due to the very high reactivity of BA, the formation of C-S-H and C-A-S-H gels proceeds faster and more prolifically for the subsequent curing phases, contributing to earlier and even farther densification of the matrix. Such kinetic advantage can provide a denser structure within the same curing period, ultimately leading to the increase of dry unit weight. Although the reference mixture integrates 0% PPF, it is inferred that the addition of PPF in other mixtures can influence the matrix density. For the specific mixture consisting of 20% BA as well as 80% FA, it can also be observed that the addition of PPF (even in lower amounts such as 0.5%) helps in bridging micro cracks and dissipating stresses within the specimen to form a much more uniform and compact matrix. On the other hand, high fiber contents might actually counteract this efficiency with more voids, but at optimal contents (for example, 0.5% PPF), these fibers improve matrix integrity without interrupting particle packing.

As per 28-day curing, compressive strength versus dry unit weight plots for GFC mixtures are shown in Fig. 7b. Positive and statistically significant strong correlation (> 0.94) have been observed. This can infer that the compressive strength probably enhances with increase in dry unit weight of those mixtures. The high value of coefficient of determination ($R2 = 0.94$) between compressive strength and dry unit weight indicates the significance of density of the matrix and coherent gel to ascertain the mechanical performance of GFC mixtures. Therefore, it has been shown that increased density due to optimized material composition and curing processes has a palpable effect on the improvement of compressive strength.

3.5 Thermal conductivity

A key component of building design and construction, thermal insulation ensures both occupant comfort and energy efficiency. Because of its distinct cellular structure, foam concrete (FC) has remarkable thermal insulation qualities [83]. The density, pore size distribution, fiber content, aggregate type, and addition of mineral admixtures are important variables that affect FC's thermal conductivity [84].

Figure 7a presents the effect of replacing FA with BA at substitution levels of 0%, 10%, and 20%, combined with PPF contents of 0%, 0.5%, and 1%, on the mean thermal conductivity of GFC mixtures prepared with 100% PA. The mixtures were subjected to initial curing at 80 °C for 24 h, followed by ambient curing for 28 days. The thermal conductivity of the GFC mixtures ranged from 0.365 to 0.619 W/mK. It is also clear that replacing FA with BA and inclusion of PPF increased the thermal conductivity. The increase in thermal conductivity brought by substituting the FA by BA accompanied with the addition of PPF occurs due to matrix densification, improved packing efficiency, and the reinforcement of heat transfer pathways by fibers as those modify porosity and strength of the material structure for efficient thermal conduction.

The highest thermal conductivity, 0.619 W/mK, was observed in the mixture containing 20% BA, and 0.5%PPF representing a 69.58% increase relative to the reference mixture. In contrast, the lowest thermal conductivity, 0.365 W/mK, was recorded in the reference mixture. At a 1% PPF content, the mixtures containing 0% and 10% BA demonstrated higher thermal conductivity compared to their counterparts with 0% and 0.5% PPF at the same BA substitution levels. It is also clear that replacing FA with BA and inclusion of PPF increased the thermal conductivity.

The replacement of FA by BA particularly at 20% creates a denser geopolymer matrix because of the much higher CaO content in BA. The reactivity is higher so C-S-H, C-A-S-H gels are formed, which contributes towards reduced porosity and more compactness of the matrix. A denser matrix would have an increased capacity for thermal conduction, which results in higher thermal conductivity [85]. BA contributes more to the solid fraction of the matrix than FA, which can have a greater percentage of unreacted particles or void-forming constituents. Indeed, the increased shape of solid material improves the pathways for conduction of thermal energy. Higher thermal conductivity is a result of the greater solid material contribution in the matrix. The addition of 0.5% PPF is going to strengthen the structure of the matrix, thus improving the joint connection of solid phases. This interconnected network allows better heat transfer through it resulting in better thermal conductivity. At 0.5% PPF, the fiber content is enough to strengthen the matrix without creating excessive voids or disruption in particle packing. For strength, it would be the mixture of 20% BA and 0.5% PPF that gives the best thermal conductivity because of both these factors that is the densification of the matrix due to BA and structural reinforcement due to PPF. Dense and well-bonded structures reduce air gaps and voids because these will be poor heat conductors; hence, conduction is improved. FA alone provides lesser reactive species for geopolymerization, thus creating a less compact matrix with more voids, inhibiting thermal conduction. The reference mixture does not possess any reinforcement that could have enhanced the thermal conduction pathways, assuming the absence of PPF. Therefore, this significantly affects the thermal conductivity, making it low. As a result, the reference mix will have the lowest thermal conductivity since it is also less dense, more porous, and has a lower degree of gel formation compared to BA-containing mixtures, about 0.365 W/mK. FA alone provides lesser reactive species for geopolymerization, thus creating a less compact matrix with more voids, inhibiting thermal conduction. The reference mixture does not possess any reinforcement that could have enhanced the thermal conduction pathways, assuming the absence of PPF. Therefore, this significantly affects the thermal conductivity, making it low.

A high coefficient of determination ($R^2 = 0.97$) indicates a strong linear relationship between dry unit weight and thermal conductivity, as shown in Fig. 8b. This strong correlation suggests that an increase in dry unit weight corresponds to an increase in thermal conductivity, which can be explained by the following structural characteristics of the material. The strong linear relationship between dry unit weight and thermal conductivity ($R^2 = 0.97$) reflects the material's structural evolution. As the matrix densify with higher dry unit weight, improved particle packing, reduced porosity, and increased solid-phase content contribute to greater thermal conductivity. This correlation highlights the influence of microstructural characteristics on the thermal performance of geopolymer foam concrete mixtures.

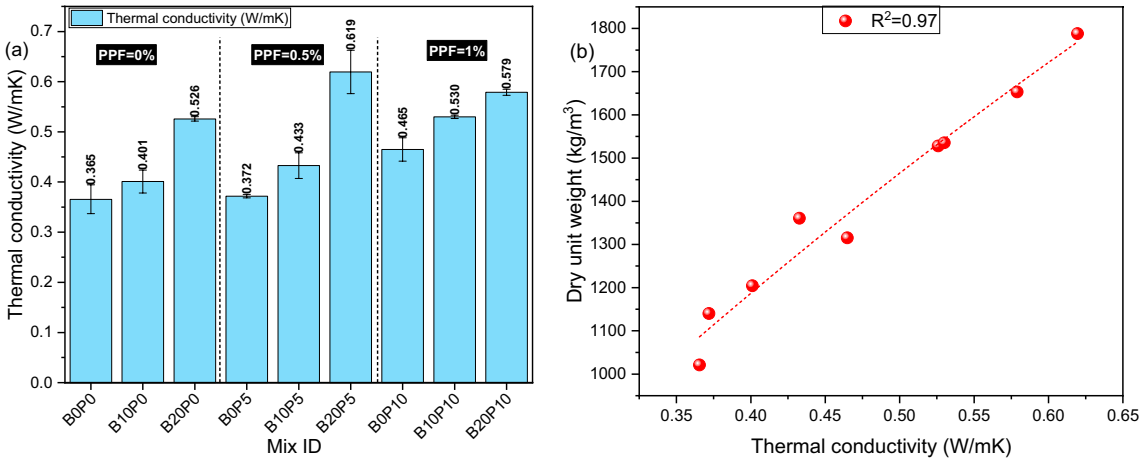

Fig. 8 **a** The results pertaining to thermal conductivity. **b** The relationship between compressive strength and thermal conductivity

 https://doi.org/10.1007/s43452-025-01369-2

3.6 The assessment of porosity and water absorption

Figure 9a presents the effect of replacing FA with BA at substitution levels of 0%, 10%, and 20%, combined with PPF contents of 0%, 0.5%, and 1%, on the mean water absorption and porosity of GFC mixtures prepared with 100% PA. The porosity of the AAFC mixtures varied between 23.82% and 47.23%, while water absorption ranged from 16.76% to 45.92%. Replacing FA with BA and incorporating PPF were observed to reduce both porosity and water absorption in the GFC mixtures. The reference mixture (100% FA and 0% PPF) exhibited the highest porosity and water absorption, whereas the mixture containing 20% BA and 0.5% PPF demonstrated the lowest values for both properties. BA has a much higher CaO content with respect to FA; hence, their presence enhances the reactivity in alkali-activated systems by producing denser binding phases such as C-S-H and C-A-S-H gels that are critical in reducing void spaces in the matrix. The denser formation of gels upon BA substitution strengthens the geopolymer network, fills micro voids, and reduces the interconnected porosity because it directly reduces water absorption. The angular and irregular shapes of BA particles improve packing efficiency by reducing the voids between the particles, which ultimately leads to a denser microstructure. FA, by contrast, has smoother, spherical particles, which contribute to higher porosity when used exclusively. The fine particle size count for BA increases its surface area, thus better distribution and packing within the matrix. This minimizes unreacted voids, further lowering porosity. The optimal geopolymerization condition is reached at 20% BA because this would be the level where the aluminosilicate content of FA and the calcium content of BA would balance. Further substitutions might result to an over-content of CaO, which could result in poor workability or even unreacted particles. PPF fibers bridge micro cracks that form during curing, thereby reducing the propagation of pores because of the influence of stress in the cohesive matrix. This can significantly improve the load transfer action within the matrix and minimizes shrinkage-induced micro cracks that tend to enhance porosity. PPF, on the other hand, is free from water absorption as it is inherently hydrophobic. When incorporated within the matrix, PPF limits the water interaction with the porous network, thereby reducing the amount of water absorption [86]. At 0.5% PPF, fiber is strong enough to reinforce the matrix without the risk of clumping or excessive voids, which is possible at higher fiber proportions. This balance plays an important role in determining the minimum rate of porosity and water absorption. FA's lower reactivity and smoother particles allow for a less densified, more porous matrix [87]. Without enough C-S-H and C-A-S-H gel formations, voids are left empty, contributing to greater porosity and higher absorption. In the absence of PPF, the matrix does not receive the merit of crack bridging and stress redistribution- inducing much micro cracking and interconnection of pores. At 20% replacement, BA shows reactivity, producing a matrix of much more density with less porosity, mainly because of enhanced formation of binding gel and more efficient packing or arrangement of particles. PPF strengthens the structural integrity

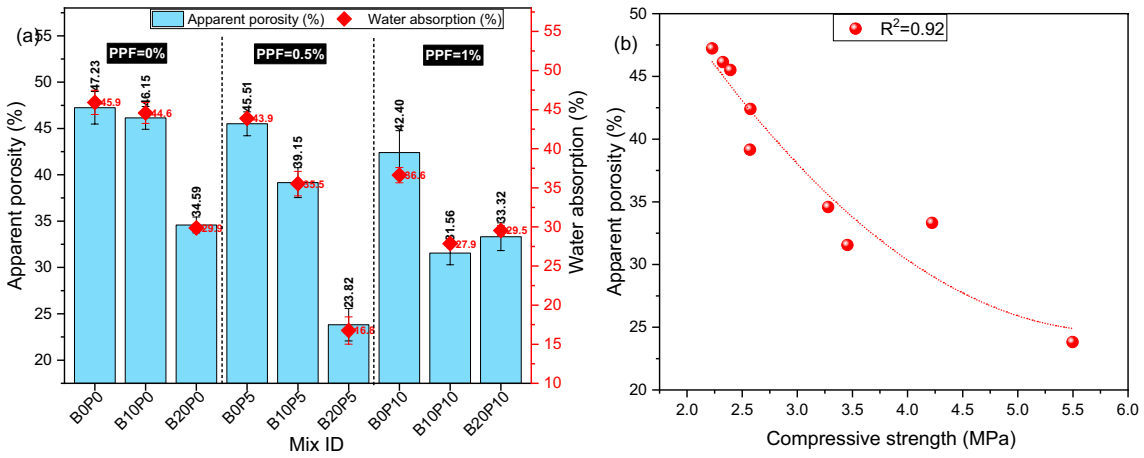

Fig. 9 **a** Water absorption vs. apparent porosity and **b** compressive strength versus porosity

of the already densified matrix through micro cracks and large interconnected voids formation. The minimum porosity and water absorption are a combined effect of these two products. Porosity is the leading factor affecting water absorption. The densification caused by BA and reinforcement by PPF not only reduced porosity but also decreased water absorption. Less interconnected porosity limits water entry into and retention in the matrix.

Figure 9b depicts the relationship between compressive strength and porosity in the tested mixtures, revealing a strong inverse correlation with a coefficient of determination ($R^2 = 0.92$). This relationship indicates that as porosity decreases, compressive strength increases,

3.7 Sorptivity

Sorptivity is the capacity of a substance to absorb water by capillary action [88]. It is a very important property for evaluating the durability of cementitious material because greater sorptivity implies increased susceptibility to moisture entry, which causes deterioration by increasing freeze-thaw damage [89], chemicals attack [90], and reinforcement corrosion [91]. Figure 10a presents the effect of replacing fly ash (FA) with boiler ash (BA) at substitution levels of 0%, 10%, and 20%, combined with polypropylene fiber (PPF) contents of 0%, 0.5%, and 1%, on the mean sorptivity of geopolymer foam concrete (GFC) mixtures prepared with 100% pumice aggregate (PA). Results show a strong correlation between sorptivity and porosity, as sorptivity in a cementitious matrix is primarily affected by the material's porosity and the connectivity of its pores [92]. The sorptivity of the GFC mixes varied between 8.28% and 28.57% highlighting a wide variation in the ability of the mixtures to absorb water. The mixture with 20% BA and 0.5%PPF, which achieved the highest compressive strength, also demonstrated the lowest sorptivity, whereas the reference mixture, which achieved the lowest compressive strength, exhibited the highest sorptivity. The utilization of BA instead of FA maximizes the generation of calcium silicate hydrate (C-S-H) and calcium aluminosilicate hydrate (C-A-S-H) gels, since BA has greater calcium oxide (CaO) content. These gels fill the empty space available in the matrix, making the entire matrix denser and decreasing the total porosity and interconnectivity of the pores created between the particles. The critical blend of 20% BA replacement causes the matrix to reach an equilibrium between geopolymerization reactions and a fairly decent particle packing, which reduces sorptivity through a dense and impervious structure. The angular and finer particles of BA, compared to spherical particles of FA, are said to be better at packing efficiency, thus reducing empty volumes even more. This improvement in packing is directly correlated to a decrease in capillary water uptake as well as lower sorptivity. PPF fibers reinforce the matrix by bridging micro cracks and eliminating discontinuities which otherwise would evolve into pathways for water. Hence, this ability to bridge cracks plays a significant role in cutting down sorptivity by breaking the continuity of capillary pores. PPF fibers are hydrophobic and,

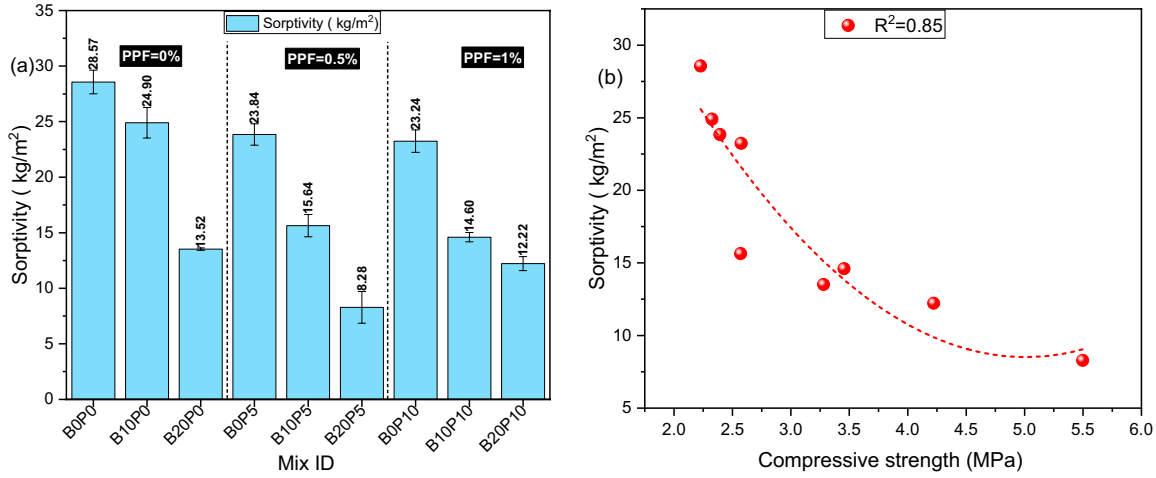

Fig. 10 **a** The results for the blends' sorptivity and **b** compressive strength vs. sorptivity

therefore, repel water and prevent capillary absorption. Hence, this characteristic puts an additional reduction in overall water absorption of the matrix, particularly seen in mixtures with 0.5% PPF, where the fiber content is optimized for structural enhancement without a lot of clustering. At 0.5% PPF, the fibers are distributed evenly within the matrix. Therefore, it effectively reinforces structure without creating too many voids or disturbance within the integrity of the matrix. This optimal content results into achieving the lowest values of sorptivity. The reference mixture has the highest sorptivity due to its porous and less cohesive structure. Spherical FA particles lead to poor packing efficiency, and since PPF is absent, micro cracks and interconnected voids are allowed to persist unbridged, promoting water absorption. The mixture that can attain the lowest sorptivity further affirms the high efficiency of BA replacement and fiber reinforcement in reducing porosity and pore connectivity. Dense gel formation, better packing of the particles, and reduced micro cracks are the factors coming together to develop a very impervious matrix. The results speak about a highly inverse correlation between sorptivity and compressive strength. While those mixtures with less sorptivity will have higher compressive strength due to lower porosity, better matrix cohesion, and better load distribution capabilities, high sorptivity will indicate a porous structure, which undermines the efficiency with which the material can carry loads in compression. Mixtures that have low sorptivity will be less prone to photographic damage due to moisture penetration, enhancing their performance against possible durability problems such as freeze-thaw cycles, chemical attack, and efflorescence [93]. These are the best mixtures for applications in the harshest environment, i.e. 20% BA and 0.5% PPF. The above results indicate the importance of BA substitution and PPF content optimization in getting a trade-off between the two properties: mechanical and durability. Bricks will crumble in time, but excess BA will lead to the brittleness of the concrete, while more PPF may create voids or clustering in it, thus compromising performance.

Figure 10b illustrates a strong inverse relationship between sorptivity and compressive strength in GFC specimens, as evidenced by the correlation coefficient of $R^2 = 0.85$. This finding suggests that as sorptivity increases, indicating greater water absorption due to higher porosity and pore connectivity, the compressive strength decreases significantly.

3.8 Dry shrinkage

Drying shrinkage occurs due to the substantial capillary pressure developed between the dry and wet regions within the micro pore network [94]. This phenomenon is activated during the completion of the geopolymeric reaction, subsequently promoting the progression of micro-crack formation [95]. Figure 11a presents the effect of replacing FA with BA at substitution levels of 0%, 10%, and 20%, combined with PPF contents of 0%, 0.5%, and 1%, on the drying shrinkage of GFC mixtures prepared with 100% PA. The drying shrinkage of the GFC

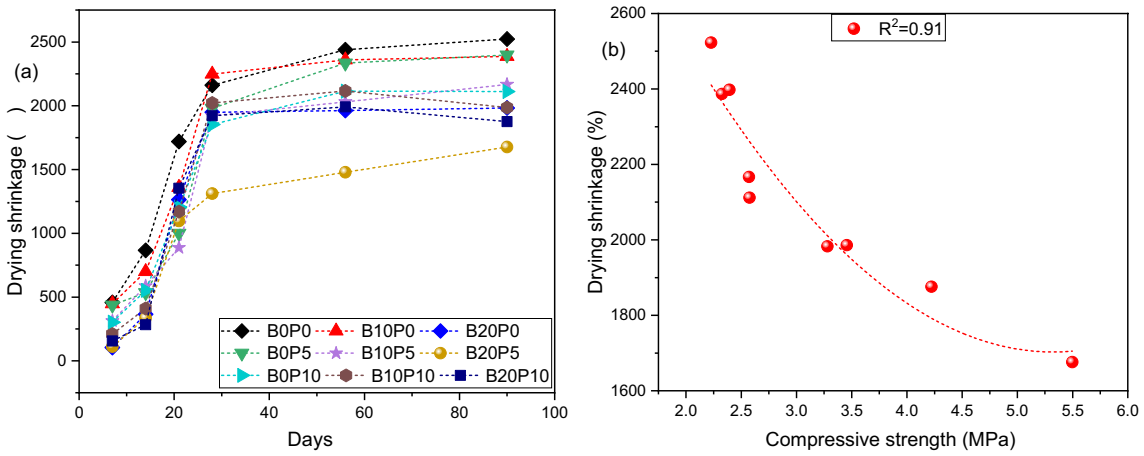

Fig. 11 Dry shrinkage outcomes of FC mixtures

mixtures was evaluated throughout a period of 90 days and ranged from values between 1876 and 2523 με by the end of the curing period. Up to 28 days, the shrinkage resulted in a quick increase in lines of the drying curve that reflected moisture loss and subsequent changes in dimensions in the early stages. Beyond that, the progress in terms of reducing the drying shrinkage became gradual and came to rest as the internal moisture levels were equilibrated over time. The early loss of moisture at an early age is significant and is due to accelerated evaporation, which causes a quick volume loss; it later becomes slow during a later period of hydration and strengthens in microstructure and therefore again becomes slow during shrinkage. The replacement of FA with BA, combined with the inclusion of PPF, effectively reduced the drying shrinkage of the GFC mixtures. Among the tested compositions, the mixture containing 20% BA and 0.5% PPF demonstrated the lowest drying shrinkage at the end of the 90-day drying period. In contrast, the reference mixture (100% FA and 0% PPF exhibited the highest drying shrinkage, emphasizing the beneficial effects of BA and PPF in mitigating shrinkage-related deformations. The inclusion of 1% PPF was observed to reduce the dry shrinkage more effectively in mixtures containing 0% and 10% BA compared to the corresponding mixtures with 0% and 0.5% PPF. However, at 20% BA, the inclusion of 1% PPF resulted in less reduction in dry shrinkage compared to the mixture with 20% BA and 0.5% PPF. This behavior highlights the importance of optimizing both the BA replacement level and PPF content to achieve the best shrinkage performance, as their interaction significantly influences the overall microstructure and drying shrinkage behavior. The blend showing 20% BA and 0.5% PPF created the smallest shrinkage at 90 days, much less than the control blend (100% FA and 0% PPF). This implies that the joint action of BA and PPF enhances stability within the matrix and also hinders shrinkage strain. The replacement of FA by BA at 10% and 20% substitution gave shrinkage reduction across all mixtures which were significant. This proves BA to be an effective pore network modifier and moisture retention reducing shrinkage because of its high calcium and reactive nature [96]. The shrinkage was reduced significantly with the addition of PPF, especially at 0.5%, as a result of distributing the shrinkage stresses and inhibiting the propagating cracks [97]. The reference mixture had maximum drying shrinkage, clearly showing the adverse effect of higher porosity, coupled with the absence of fiber reinforcement. This shows that both BA replacement and PPF inclusion are important for the shrinkage resistance. The drying shrinkage curves indicate that most drying shrinkage occurs very rapidly within the first 28 days, followed by a more gradual increase in shrinkage until 90 days. This indicates that there is a loss of capillary water within the material in the early days, followed by contraction of the gel structure. Both the BA and PPF modifications were effective not only in minimizing early shrinkage but also in controlling shrinkage in later ages.

Figure 11b reveals a strong inverse relationship between compressive strength and drying shrinkage, as indicated by a high correlation coefficient ($R^2 = 0.91$). The findings emphasize that improving the compressive strength of GFC mixtures also positively impacts their shrinkage resistance, making the materials more suitable for long-term structural applications.

3.9 Microstructural changes after 28 days curing period

The SEM picture of the reference composite B0P0 (100% FA, 0% BA, and 0% PPF) shown in Fig. 12a is crucial for microstructural understanding related to poor macroscopic performance. FA particles show spherical shape in the SEM image, which is responsible for lack of interlocking between these particles. For absolute comparison, unlike angular particles like BA, spherical FA will give rise to a loose packed matrix with increase in voids, thus reducing overall densification. The largest unfilled voids dominate the matrix structure as seen in the image. Voids thus contribute to increased porosity and thus reduce mechanical strength and durability. The smooth surface of FA particles as seen in the SEM image, indicated that these particles had very little reaction or geopolymerization. This observation and the lesser reactivity of FA relative to BA thus lead to lesser binding gels to fill the voids and augment cohesion. In connection with these observations of not interpreting visible binding phases in terms of C-S-H or C-A-S-H gels lacks geopolymerization. Therefore, it is not capable of yielding the requisite dense gel matrix for structural integrity, when only using FA. Unreacted FA particles occur prevalently in the SEM image; this indicated that the alkaline activator, could not mobilize the whole aluminosilicate within FA

 https://doi.org/10.1007/s43452-025-01369-2

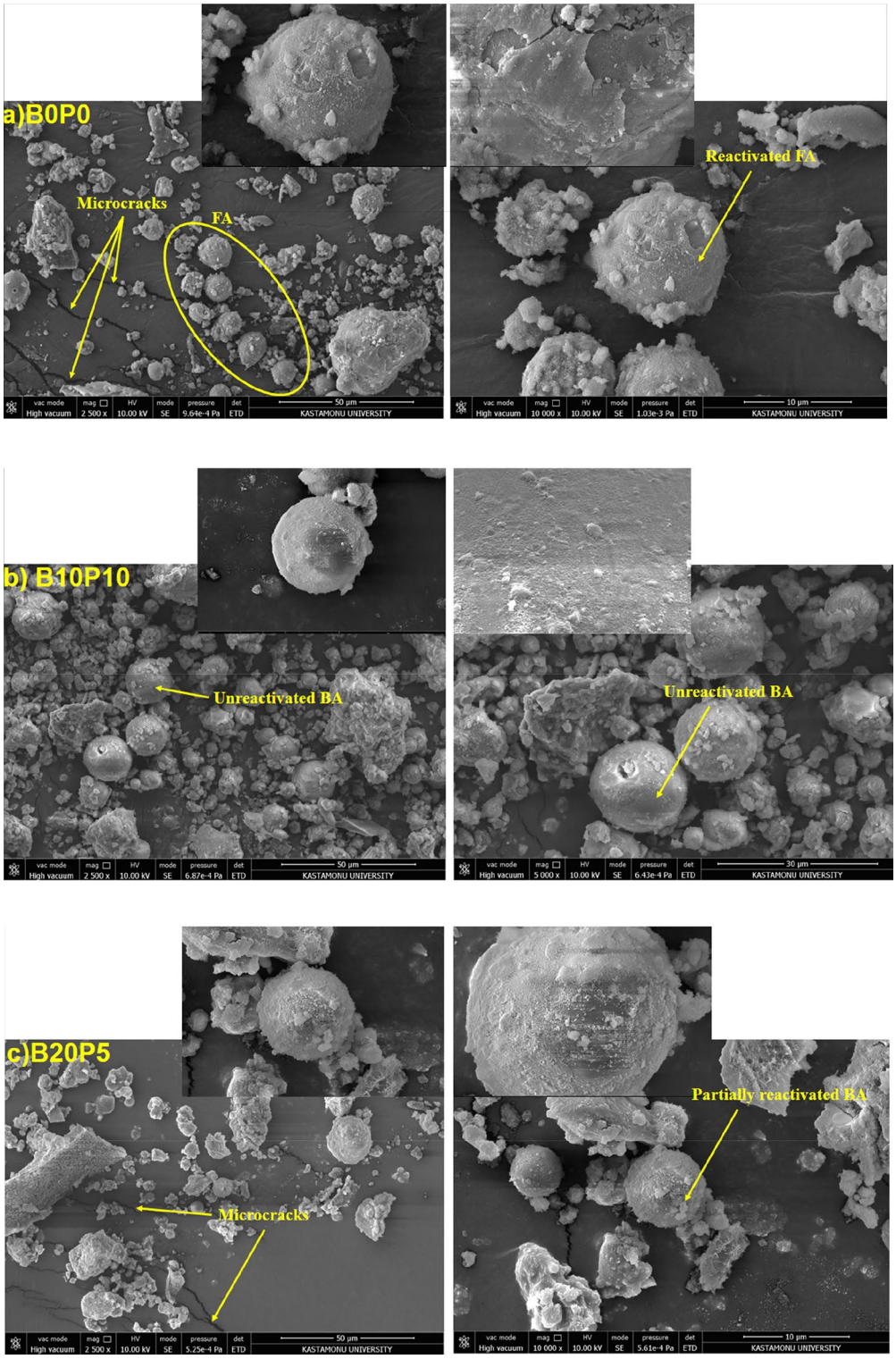

Fig. 12 Microstructures of specimens after 28 days curing period **a** B0P0 **b** B10P10 **c** B20P5

[98]. Thus, it would be responsible for the matrix having poor mechanical performance and high water absorption capacity. Fine micro cracks are visible in the SEM image which most probably cause shrinkage during curing or external stresses. Without the PPF, the structural integrity of the matrix is compromised by these cracks remaining unbridged. The SEM image indicates a considerable degree of interconnected porosity, which is consistent with the high sorptivity and proneness to water ingress of the mixture. This quality is likely to increase the possibility of freeze-thaw damage and chemical attack. The packing of FA particles is very loose as it contains no binding gels, which leads to this mixture being compared with all other mixtures to having the lowest compressive strength. The weak interactions between particles cannot withstand any applied stresses and therefore tend to fail somewhat prematurely. The high porosity and corresponding high sorptivity values for this mixture correlate with visible voids lacking densification. Hence, it allows the easy entry of water into the matrix to bring about durability problems within the life of the concrete. Low dry unit weight results from absence of dense gel forms and existence of voids. Here again, this shows the incapacity of the matrix to form a coherent matrix. In other mixtures with BA contents, SEM images would show a denser microstructure because of the angular and irregular BA particles that promote packing and gelling among particles. The absence of these two critical benefits from B0P0 is caused by the absence of BA from it. The benefit of PPF in mixtures is reduction in the cracks produced along with an effective stress distribution. This gives cracks, however, in the absence of PPF in B0P0 unbridged matrices that allow cracks to extend and further weaken the structure.

The SEM image of mixture B10P10 (90% FA, 10% BA, and 1% PPF) shown in Fig. 12b presents a microstructure with significantly improved densification, gel formation, and reinforcement compared to the reference mixture (B0P0).The SEM image shows a combination of spherical FA particles with angular BA particles. This heterogeneity essentially promotes particle packing since it allows the angular particles to fill the voids left by the spherical ones and greatly decrease porosity while increasing matrix density. The angular BA particles offer interlocking structure within the matrix and, of course, improved cohesion and strength. It is a sharp contrast with the looser packing in B0P0, which depended solely using FA. The interaction of FA and BA particles would probably be that of cohesion since the reaction products bound them together into a denser microstructure, which is in the order of optimized ratio among the aluminosilicates from FA and calcium oxide (CaO) from BA. The SEM image probably shows binding phases such as calcium silicate hydrate (C-S-H) and calcium aluminosilicate hydrate (C-A-S-H). These gels act as bridges between particles thus decreasing porosity increases compressive strength. At 10% replacement, BA contributes a sufficient quantity of reactive CaO that promotes formation of gel not flooding the matrix, which would cause shrinkage or unreacted particles. The final product is thus balanced geopolymer matrix with fewer voids. Some portions of the SEM micrograph are thick gels which indicate areas of very effective geopolymerization. These regions add crucial significance to the overall strength and decreased porosity of the matrix. The SEM image also show PPF fibers filling the matrix space, linking micro cracks while suppressing crack extension and hence reducing chances of water getting into durability related issues such as mechanical failure. The fibers, at 1% dosage, are well dispersed enough to improve the fracture without forming clumps or leaving voids that would happen with a higher dosage of fibers. The SEM image shows fibers embedded between the matrix with very dense binding gels; thus, indicating stronger bonding and matrix for effective load transfer and stress distribution. Except for a few voids, interconnectivity showed fewer readings as compared to B0P0. This is the direct result of the reduction in porosity correlating to reduced sorptivity and water absorption of B10P10, as discussed in Sect. 3. This effectively produces a matrix with pores that are relatively closed, thus, enhancing water resistance and durability. The closure of these pores would, therefore, be highlighted in the SEM image as regions of improved integrity. Furthermore, according to the results from the SEM image, there would be fewer cracks visible as a result of resistance to micro crack propagation, fiber reinforcement, and improved gel formation in the composite. With denser and lower pore structure, it will resist better to freeze and thaw cycles compared to the previous because of minimized water ingress and covered brittle existing cracks. This gives a better gel structure along with reduced porosity to protect the matrix from chemical attack due ingress of aggressive agents.

The SEM image of B20P5 (80% FA, 20% BA, and 0.5% PPF) shown in Fig. 12c illustrates the microstructural features that contribute to the superior performance of this composition. The image probably indicates the complementarity between the spherical FA particles and the angular BA particles; the angular BA particles fill the interstitial spaces between the smoother FA particles, increase packing density, and attain minimum voids due to space filling. Replacement of FA with BA by 20% meets the required balance between the reactivity of the particles and the level of packing efficiency achieved. This would lead to increased shrinkage or unreacted particles if the BA content is increased; however, a lower amount does not provide enough reactive calcium oxide (CaO) for effective gel formation. The dense zones confirmed in the SEM image indeed indicate a matrix with the least unfilled spaces, which correlates to highest dry unit weight and lowest porosity for B20P5. The SEM image here likely depicts some presence of these binding gels, forming due to reactive CaO from BA and aluminosilicate from FA. These form bridges between the particles filling voids and contributing to the strength and durability of the matrix. Seeing this homogenous distribution of binding gels as a smooth and cohesive texture in the SEM image indicates geopolymerization effectiveness, ensuring that loads are uniformly distributed and that weak points are reduced. The high extension of gel formation seen in the SEM image goes hand in hand with the highest compressive strength of B20P5. A structure dense and well-bonded can sustain applied loads without cracking. The fibers bridging the matrix's micro cracks are probably visible in the SEM image. By efficiently stopping cracks from spreading, these fibers improve the material's resilience to external damage and mechanical stress. The 0.5% PPF concentration provides adequate reinforcement without creating extra voids or fiber clustering, striking a balance. The uniformly distributed fibers visible in the SEM scan make this clear. By improving the matrix's capacity to transfer stress, fibers lessen the concentration of localized stresses that might contribute to failure. The SEM image probably depicts more closed voids than interconnected porosity. Among the mixes, these closed pores have the lowest sorptivity because they minimize water infiltration. Because of the lack of pore connection, the matrix is more durable in hard environmental conditions because moisture and hostile chemicals cannot readily pass through it. The small, closed spaces seen in the SEM image match B20P5's stated lowest sorptivity, guaranteeing superior resistance to freeze-thaw damage and water absorption. It appears from the SEM image that the particles, gels, and fibers are uniformly dispersed throughout the matrix. Because of its homogeneity, the mixture's outstanding performance is attributed to the material qualities remaining constant throughout. According to the SEM image, there is a strong bond between the FA and BA particles and the surrounding gels. The mixture's mechanical qualities and durability are improved by this strong interfacial bonding. The SEM picture of B20P5 reveals a denser matrix with fewer gaps and more widespread gel formation than that of B10P10. In terms of durability and compressive strength, this explains why B20P5 performs better than B10P10. High porosity, inadequate particle packing, and little gel formation were all visible in the B0P0 SEM picture. B20P5, on the other hand, exhibits a cohesive, gel-filled matrix with efficient fiber reinforcing, leading to better qualities. The maximum compressive strength attained by B20P5 is directly supported by the dense and tightly packed microstructure seen in the SEM image. The cohesiveness and compactness of the matrix are a reflection of the minimal voids and dense packing, which result in the biggest dry unit weight. Since there are no linked pores, B20P5 has the lowest sorptivity and porosity, which makes it resilient to water intrusion and long-lasting in challenging environments.

3.10 Durability of the blends under high temperatures

3.10.1 Compressive strength

Figure 13a illustrates the influence of replacing FA with BA at substitution levels of 0%, 10%, and 20%, in combination with PPF contents of 0%, 0.5%, and 1%, on the average compressive strength of GFC mixtures containing 100% pumice aggregate (PA) after 28 days of curing and subsequent exposure to elevated temperatures. The mixtures were subjected to initial curing at 80 °C for 24 h, followed by ambient curing for 28 days. Figure 13b compares the compressive strength of mixtures cured for 28 days with those subjected to temperatures

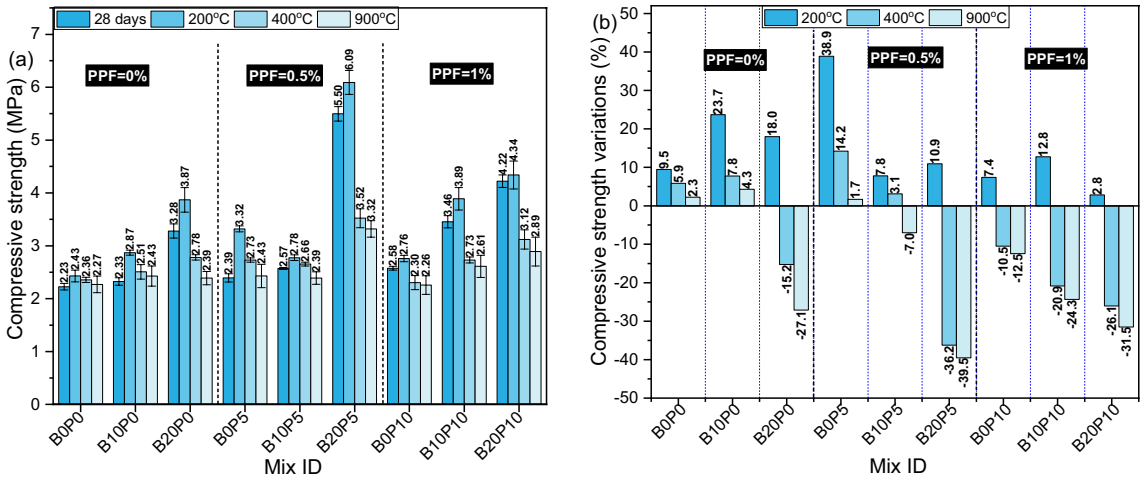

Fig. 13 **a** The effects of high temperatures on compressive strength and **b** changes in strength

ranging from 200 °C to 900 °C. The results demonstrate that all mixtures exhibited an increase in compressive strength after exposure to 200 °C, with enhancements varying from 2.8% to 38.9%. The lowest strength gain was observed in the mixture containing 20% BA and 1% PPF, while the highest increase occurred in the mixture with 100% FA and 0.5% PPF. These findings highlight the interplay between material composition and thermal exposure in influencing the mechanical properties of GFC. The matrix becomes denser and less porous when heated to 200 °C because any remaining moisture evaporates. This procedure strengthens the linkages inside the geopolymer matrix, increasing compressive strength. Especially in alkali-activated systems, moderate heat can speed up unreacted components even further, increasing their strength. Due to the spherical particle shape of FA and its pozzolanic activity, which help to produce a dense, cohesive matrix under thermal activation, the 100% FA mixture with 0.5% PPF had the greatest strength improvement [99]. The consistent geopolymerization and workability are improved by the spherical particles' reduction of internal friction. Fiber distribution successfully strengthens the matrix at 0.5% PPF without adding too many voids. Rapid gel formation (C-S-H and C-A-S-H) is caused by the angular particles and high calcium content of BA. However, the angular particles cause micro cracks and decrease workability at 20% BA and 1% PPF. It seems that increasing PPF and BA content decreased the high temperature resistance of the mixture. At 0%PPF content, the mixtures with 0 and 10%BA also exhibited strength gain at 400 and 900 °C but the mixture with 20%BA exhibited strength loss of 16.2 and 27.1% at 400 and 900 °C respectively.

When temperatures rise over 160–170 °C, PPF starts to break down and begins to burn off at 400 °C, leaving gaps in the matrix [73]. These spaces impair the material's structure, increase porosity, and lower its overall mechanical strength-especially when PPF is heavily involved in reinforcing the geopolymer matrix. PPF completely degrades and turns into a more porous and brittle substance by 900 °C [100]. The lack of PPF's crack-bridging ability makes the geopolymer matrix more vulnerable to shrinkage and heat stress. Due to its high calcium oxide (CaO) content, BA helps produce C-S-H gels, which improve the material's initial strength. However, the excess calcium quickly shrinks, micro cracks, and degrades the matrix when exposed to high temperatures like 400 °C and 900 °C. Calcium oxide levels rise with increasing BA content, hastening shrinkage and cracking at high temperatures. Because of these destabilizing effects, the mixture exhibits a notable loss of strength at 20% BA (16.2% at 400 °C and 27.1% at 900 °C). The geopolymer network is upset by too much calcium, which makes the material more brittle and vulnerable to heat stress damage. A more brittle matrix is produced at high temperatures when the PPF and BA contents are increased. Although PPF offers reinforcement at first, the material's resistance to heat stress is diminished when it degrades at high temperatures. However, by adding too much calcium, BA makes the material more brittle, which, along with the loss of PPF reinforcing,

seriously reduces the material's resistance to high temperatures. The extra calcium causes increased thermal instability and shrinkage at 20% BA, and when paired with PPF degradation, the mixture loses a significant amount of strength. Under heat stress, the material becomes more porous and more likely to crack, which results in the strength reductions that have been observed.

At a PPF content of 0.5%, the mixture containing 0% BA (100% FA) demonstrated a strength gain at both 400 °C and 900 °C. In contrast, the mixture with 10% BA showed a strength gain at 400 °C but experienced a 7% strength loss at 900 °C. Meanwhile, the mixture with 20% BA exhibited the most significant strength loss at both 400 °C and 900 °C among all the tested mixtures. The steady pozzolanic reactions of FA and the reinforcing impact of PPF, which give improved structural integrity, are responsible for the strength gain at 400 °C and 900 °C for the 0% BA (100% FA) mixture. The 10% BA mixture gains strength at 400 °C because of partial sintering, but at 900 °C it becomes unstable because of PPF breakdown and too much calcium. At both temperatures, the 20% BA mixture exhibits the greatest strength loss, mostly as a result of the excess calcium oxide, which causes shrinkage, micro cracking, and decreased thermal stability. Conversely, at a PPF content of 1%, all mixtures exhibited a reduction in strength at both 400 °C and 900 °C. This strength loss became more pronounced with the increase in BA content. High temperatures (over 160–170 °C) cause PPF to degrade, creating gaps in the matrix that increase porosity and weaken the material. Complete PPF degradation weakens the matrix much more at 900 °C. Although the higher calcium oxide (CaO) content of boiler ash (BA) encourages the development of C-S-H gels, it also weakens the material by shrinking, micro cracking, and thermally degrading at high temperatures [101]. Greater strength loss results from the material being more brittle due to the combination of PPF breakdown and high BA content. Micro cracking increases and the matrix becomes more brittle as a result of this synergistic action.

3.10.2 Weight loss

Figure 14a illustrates the effect of replacing FA with BA at substitution levels of 0%, 10%, and 20%, in combination with PPF contents of 0%, 0.5%, and 1%, on the average weight loss of GFC mixtures containing 100% PA after exposure to elevated temperatures. The experimental results indicate that all GFC mixtures experienced weight loss upon exposure to high temperatures, with the rate of weight loss increasing progressively as the temperature was raised [102].

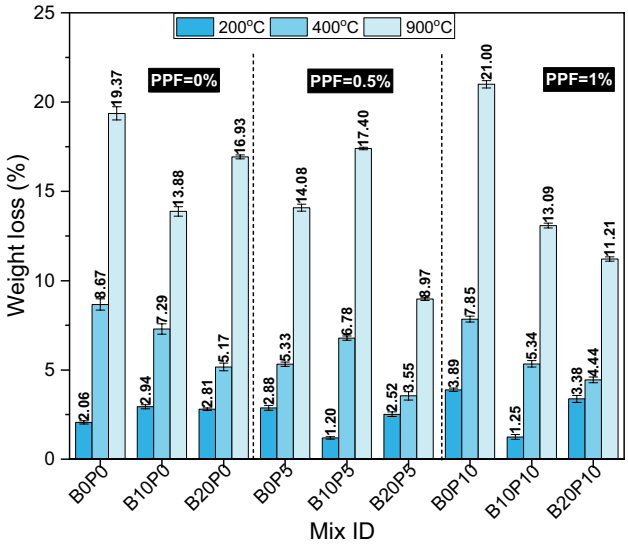

Fig. 14 Loss of weight when exposed to high temperatures

At 200 °C, the mixture containing 10% BA and 0.5% PPF exhibited the lowest weight loss, while the mixture with 0% BA (100% FA) and 1% PPF demonstrated the highest weight loss. The weight loss observed at 200 °C was primarily due to the evaporation of moisture in the mixtures [103].

In comparison to FA, BA has a larger percentage of calcium oxide (CaO). By reducing porosity, BA helps to create more stable geopolymeric gels at 200 °C, like calcium silicate hydrate (C-S-H), which improve the material's structural integrity and lessen weight loss [104]. The mixture's higher calcium concentration helps to reduce weight loss by retaining more moisture and preventing excessive evaporation [105]. When PPF starts to break down at 200 °C, its burning off increases porosity and decreases material density. Because 1% PPF degrades more readily and there is less calcium to support the geopolymer matrix due to the absence of BA, the mixture containing 0% BA (100% FA) and 1% PPF shows the greatest weight loss. This makes the material more susceptible to moisture loss.

At 400 °C, the reference mixture containing 0% BA and 0% PPF exhibited the largest weight loss, while the mixture with 20% BA (80% FA) and 0.5% PPF demonstrated the lowest weight loss. The reference mixture with 0% BA and 0% PPF loses the most weight at 400 °C because it lacks the stabilizing effects of BA and the reinforcement of PPF, leaving it extremely vulnerable to moisture loss and thermal degradation [106]. The mixture containing 20% BA (80% FA) and 0.5% PPF, on the other hand, shows the least amount of weight loss because the BA reduces moisture loss and offers thermal stability, while the moderate PPF component preserves matrix integrity without creating too many voids. Weight loss is limited and the mixture's resistance to high temperatures is improved by the addition of BA and a moderate quantity of PPF. At 900 °C, the mixture containing 0% BA and 1% PPF exhibited the largest weight loss, while the mixture with 20% BA (80% FA) and 0.5% PPF demonstrated the lowest weight loss. The mixture containing 0% BA and 1% PPF loses the most weight at 900 °C because the fibers completely decompose, creating a significant number of voids that increase porosity and let more moisture escape. The mixture containing 20% BA (80% FA) and 0.5% PPF, on the other hand, shows the least amount of weight loss because the stabilizing effect of BA decreases shrinkage and cracking, and the moderate PPF content reduces the number of voids, which improves moisture retention and reduces losing weight. At high temperatures, the combined actions of BA and regulated PPF content result in improved thermal stability and less weight loss.

3.10.3 Microstructural changes after 900 °C

The SEM image of reference mixture B0P0 (100% FA, 0% BA, and 0% PPF) captured after thermal exposure at 900 °C indicates enormous microstructural modifications attributed to thermal exposure (Fig. 15a). In fact, even though here there is only a mere gain of 2.3% in compressive strength, the microstructure vulnerable as it loses the second greatest weight among all mixtures tested. In the SEM image, it shows the non-reactive FA particles that take the longest time to observe retention of spherical FA particles, as there would not be much binding phase development (for example, C-S-H or C-A-S-H gels). The rest of the matrix still comprises loose and poor packing of the particles. Micro cracks and voids are visible in the SEM image due to different thermal expansion and shrinkage patterns of the matrix components. These structural deficiencies increase the porosity and reduction of cohesion within the matrix. At 900 °C, thermal stress causes the weak sections to break; such mechanics can be seen in SEM micrographs as fragmented aspects. This loss in weight can be attributed to evaporation of physically and chemically bound water and decomposition of small portions of binding gels that were formed during early curing. The matrix does not possess calcium-based gels which are quite thermally stable, being formed in the painting process without BA, showing an increased weight loss or porous development and more structural degradation. This little increase in compressive strength (by 2.3%) could be due to sintering at very localized sites, where some of the FA particles were joining together at high temperatures, forming a more densely packed arrangement of the particles at some locations. The small agglomerated or fused regions which may probably have caused this effect can be seen in the SEM image. The SEM image shows that the matrix is porous and weak due to the lack of BA and PPF, which restricts the amount of densification. A very porous and linked network of voids is probably visible in the SEM image. Weight loss is facilitated by this porous structure, which also lowers

 https://doi.org/10.1007/s43452-025-01369-2

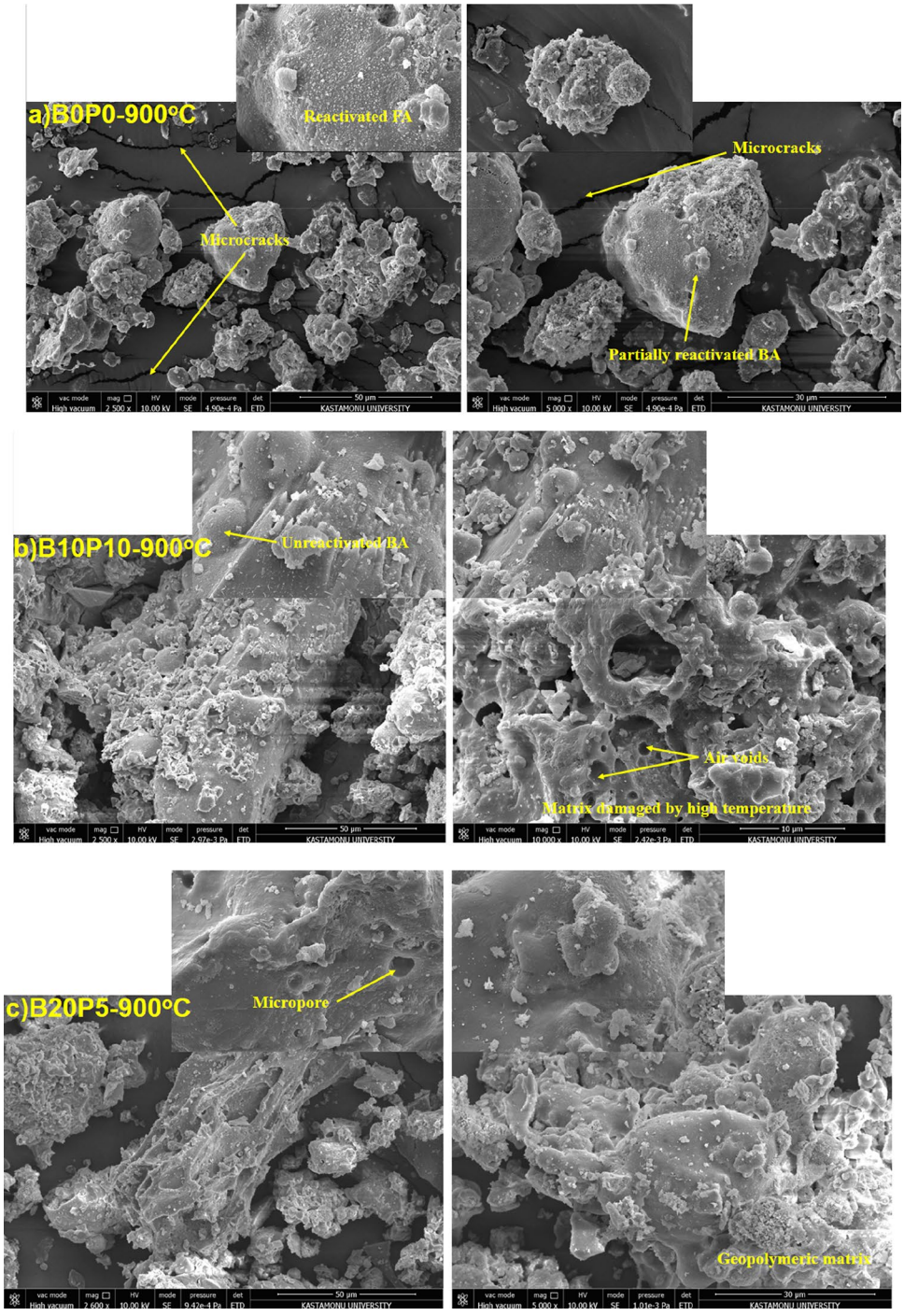

Fig. 15 Microstructure of specimens exposed to high temperature (900 °C) **a** B0P0 **b** B10P10 **c** B20P5

the material's thermal resistance. Greater permeability is made possible by the linked porosity, which reduces the mixture's durability and increases its susceptibility to environmental deterioration after exposure.

The SEM picture of mixture B10P10 (90% FA, 10% BA, and 1% PPF) following exposure to 900 °C sheds light on the microstructural alterations and performance as shown in Fig. 15b. In comparison to similar combinations with 10% BA but lower or no PPF concentration, which performed better, this mixture showed considerable heat degradation with a loss of compressive strength of 24.3%. A somewhat broken and cracked matrix is probably seen in the SEM image. Micro cracks that jeopardize the matrix integrity are caused by shrinkage and thermal expansion mismatches brought on by the high thermal pressures at 900 °C. PPF fibers thermally decompose

and evaporate at high temperatures, leaving behind micro spaces that weaken the matrix, which is why the voids in the SEM image are apparent. The SEM image shows loose particle arrangement and reduced densification, which indicate partial degradation of the binding phases (C-S-H and C-A-S-H gels) created by BA inclusion. The incapacity of the matrix to adequately withstand stress is a result of PPF's lack of reinforcing function during thermal breakdown. When compared to combinations with no or minimal PPF concentration, this is the main cause of the notable 24.3% loss in compressive strength. PPF vaporization creates tiny gaps that show up as hollow areas in the SEM picture. The load-bearing capability of the matrix is decreased by these spaces, which increase porosity. The mixture without PPF showed a 4.3% strength boost, which suggests that its simpler matrix structure is more stable in hotter temperatures. PPF prevents voids from forming as a result of fiber deterioration, enabling the matrix to sinter and mildly densify. This mixture's decreased fiber content reduces void formation while still offering some limited crack-bridging benefits at lower temperatures, as evidenced by the smaller strength loss (7%) for this mixture. Because of the higher fiber breakdown, the SEM image for B10P10 would probably display a larger void network than the 0.5% PPF mixture. The SEM picture most likely shows weaker gel phases as a result of exposure to high temperatures. At 900 °C, the binding efficiency of these gels (C-S-H and C-A-S-H) decreases, resulting in a more porous structure. By creating thermally stable calcium-based gels, the 10% BA component increases heat resistance when compared to combinations without BA. The substantial heat damage brought on by PPF deterioration, however, limits BA's contribution. Due to PPF breakdown and thermal cracking, the SEM picture displays a very porous structure. The observed strength loss is partly caused by the linked pores, which also lower the matrix's mechanical performance. Increased porosity jeopardizes the matrix's long-term durability by increasing the likelihood of water intrusion, chemical attack, and freeze-thaw damage. Micro cracks created by thermal expansion and the lack of fiber reinforcement following PPF deterioration are seen in the SEM picture. The ability of the matrix to evenly distribute stresses is diminished by these fissures. Degraded PPF and weakening gels work together to create high-stress concentration areas that appear as fragmented regions in the SEM picture.

SEM image of mixture B20P5 (80% FA, 20% BA, and 0.5% PPF) reveals that after thermal exposure to 900 °C, an intense thermal degradation process has occurred and among all tested mixtures, this composite has the maximum compressive strength loss with 39.5% loss (Fig. 15c). This was compared with those having the same BA mixture but different PPF dosage (0% or 1%) where smaller reductions in strengths can be observed. SEM Reveal extensive micro cracking which develop under thermal induced stresses due to contraction of the matrix components. The cracks propagate unrestrained and are the result of very limited reinforcement afforded by 0.5% PPF dosage. The image likely presents weakened or partially degraded C-S-H and C-A-S-H gels. Although 20% addition of BA improves gel formation at ambient conditions, these gels are thermally unstable and undergo degradation at 900 °C, causing voids and thus weakening the matrix. At 900 °C, PPF fibers experience such degradation and emerge as micro voids. Though the 0.5% dosage might create less micro voids compared to higher fiber contents (1%), still these micro voids would reduce the density of the matrix in load carrying capacity. The SEM image might represent limited crack-bridging effects due to low PPF content (0.5%). Though the microfibers give some resistance to micro crack development, the reinforcement is too low to neutralize the severe cracking due to thermal stresses. Mixtures with 1% PPF give lower strength loss (31.5%) since more fibers are available for bridging and lessening the intensity of cracks. The SEM image of B20P5 shows less effective actions against cracking compared to an equivalent 1% PPF. Strength loss of 27.1% is shown by the combination of 20% BA and 0% PPF, which is attributed to the incomplete void formation caused by fiber decomposition. This means that though fibers provide some capability to manage cracks, their thermal degradation is detrimental to the matrix if not handled properly. The SEM micrograph exhibits an extremely porous structure with empty voids formed by the decomposition of the gel and by the fibers. Consequently, such voids interconnect and in turn decrease matrix density and compressive strength. The simultaneous degradation of binding gels with that of the fibers worsens porosity, as seen in the SEM image that reveals massive voids and regions of unbounded particles. Moreover, contribution by 20% BA increases the initial gel formation in the form of C-S-H and C-A-S-H. These gels, however, are thermally unstable, decomposing at high temperatures of 900 °C to leave behind a weakened structure.

It is very likely that the SEM image shows the remnants of gels in fragmentary or degraded state. BA enhances high-temperature performance to some extent but then all the positive effects disappear with the advent of excessive gel degradation at 900 °C, as seen in the disorganized matrix of the SEM image. However, in the 0% PPF mixture, there is reduced strength loss (27.1%) due to the absence of void formation from fiber decomposition; however, it results in poor management of cracks because the matrix is not optimally designed to resist thermal stress. The optimal higher PPF dosage in the 1% PPF mixture enhances crack resistance, decreasing the strength loss up to 31.5%. The SEM image of B20P5 with 0.5% PPF shows less fibers bridging cracks proving that the minimal dosage has limitations. B20P5 loses 39.5% of its compressive strength as a result of severe heat cracking, gel deterioration, and void formation. The structural flaws that appear when exposed to heat are confirmed by the SEM image. A crucial factor is striking a balance between fiber reinforcement and fiber-induced void formation. When the fibers degrade, they leave behind holes that cannot be filled by the fibers at 0.5% PPF. The very porous and fractured structure seen in the SEM image suggests a decreased ability to withstand chemical attack, moisture intrusion, and freeze-thaw cycles. The matrix's capacity to withstand high temperatures or cycle conditions is jeopardized by the microstructural deterioration seen in the SEM image.

4 Exposure to freeze-thaw cycles

4.1 The compressive strength

Figure 16a shows the impact of replacing FA with BA at substitution levels of 0%, 10%, and 20%, combined with PPF contents of 0%, 0.5%, and 1%, on the average compressive strength of GFC mixtures containing 100% PA after 28 days of curing and exposure to 15 and 30 freeze-thaw (F-T) cycles. Figure 16b displays the variations in compressive strength of the mixtures after 15 and 30 F-T cycles. As shown in Fig. 16, all mixtures exhibited an increase in compressive strength following 15 F-T cycles, with strength gains ranging from 5.28% to 50.58%. The main chemical reaction that creates a durable matrix in geopolymer mixes during the curing process is the reaction of aluminosilicates (such as fly ash or boiler ash) with alkaline activators. Over time, this matrix gets stronger and more compact. The intrinsic stability of the geopolymer matrix aids in resistance to damage even after exposure to F-T cycles, which enhances strength under regulated circumstances [107].

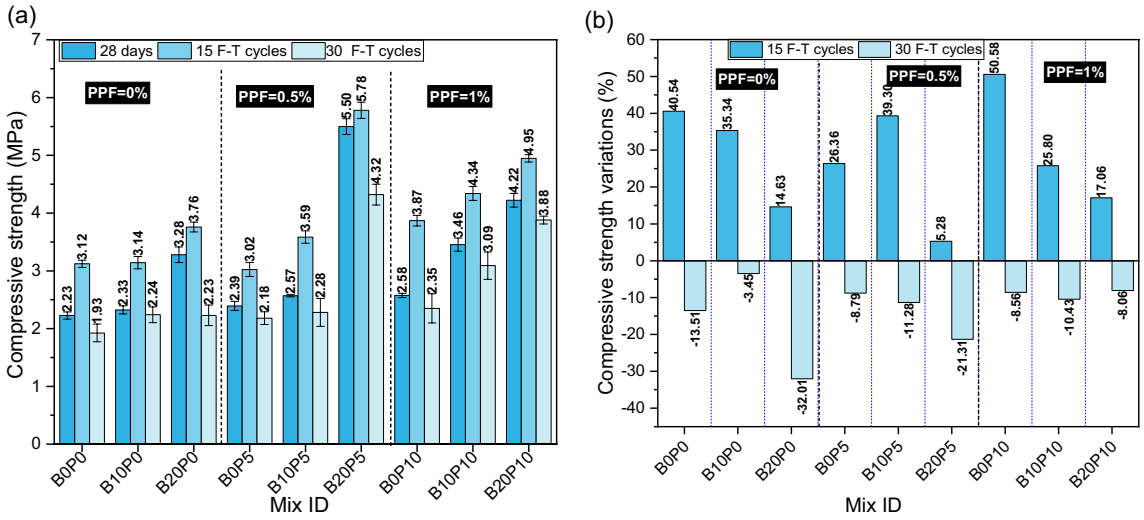

Fig. 16 Compressive strength values (**a**) and strength fluctuations (**b**) following F-T cycles

Even when exposed to freeze-thaw conditions, geopolymers usually become stronger over time as the polymerization process proceeds. As the matrix "matures" and becomes more resilient, the addition of FA and BA to the mixture promotes the development of a denser and more cohesive structure, which could increase strength. During F-T cycles, water trapped in the material's pores expands when frozen and contracts when thawed. This process might produce an initial densification of the geopolymer matrix as it adjusts microscopically to accommodate the stresses caused by freezing and thawing. For some mixes, this process can boost inter particle bonding and cohesion inside the matrix, resulting in higher strength.

Initially, the F-T cycles may cause microscopic micro cracks to appear in the material. In some situations, these fissures may relieve internal stresses within the matrix, allowing for better force distribution and stress transmission inside the material, thus contributing to an improvement in strength. Additionally, as the geopolymer matrix stabilizes, minor cracks can be "healed" by continued geopolymerization, leading to improved mechanical properties [108].

The mixture containing 0% BA (100%FA) and 1% PPF exhibited the largest strength gain, while the mixture with 20% BA (80% FA) and 0.5% PPF demonstrated the lowest strength gain after 15 F-T cycles. The mixture with 0% BA (100% FA) and 1% PPF had the greatest strength improvement because the fiber reinforcement (1% PPF) effectively mitigates the damage caused by freeze-thaw cycles [109], and the absence of BA assures a more stable geopolymer matrix that resists shrinkage and cracking. In contrast, the mixture with 20% BA (80% FA) and 0.5% PPF had the lowest strength improvement because to the high BA content, which causes shrinkage and brittleness, and the low PPF content, which provides less protection against freeze-thaw-induced cracking [110]. The material's high BA and low fiber content rendered it more susceptible to freeze-thaw degradation, limiting its strength gains.

On the other hand, all mixtures exhibited strength loss with strength loss ranging from 3.45% to 32.01% after 30 F-T cycles and the mixture containing 20% BA (80%FA) and 0% PPF exhibited the largest strength loss, while the mixture with 10% BA (90% FA) and 0% PPF demonstrated the lowest strength loss. BA includes a substantial amount of calcium oxide (CaO), which promotes the production of C-S-H (calcium silicate hydrate) gels, hence increasing the strength of geopolymer materials. However, when the BA content exceeds a specific level, particularly in the 20% BA mixture, the high calcium content causes brittleness, shrinkage, and thermal instability. During freeze-thaw cycles, the material shrinks and micro cracks due to the expansion of water in the pores during freezing and contraction during thawing, resulting in increased strength loss. When compared to the 20% BA mixture, the 10% BA (90% FA) mixture has a reduced calcium concentration, which lessens brittleness. The decreased calcium oxide level reduces the material's susceptibility to shrinkage and cracking during freeze-thaw cycles, resulting in improved thermal stability and strength retention. As a result, the 10% BA mixture has the lowest strength loss (3.45%), as the lower calcium level reduces shrinkage and micro cracking. Although the mixtures presented here do not contain PPF, it is crucial to highlight that the lack of PPF in both mixtures means that their performance is totally dependent on the material composition. The 10% BA mixture still works better because the balance of FA and BA results in a more stable matrix, whereas the 20% BA mixture suffers more from thermal instability induced by the high calcium level. During the freeze-thaw cycles, water trapped in the material expands when frozen and contracts when thawed. This leads to the internal stresses from such expansion and contraction, which may result in cracking if the material fails to absorb the stress. Concerning the 20% BA mixture, the high ratio of calcium promotes shrinkage and makes it more brittle, hence making this particular mixture prone to cracking and greater loss in strength as a result of freeze-thaw. A 10% BA mixture would result in a comparatively lower internal stress build-up during freeze-thaw cycles, thus leading to limited shrinkage and micro cracking due to reduced calcium content, thereby improving strength retention and reducing damage from freeze-thaw cycles.

 https://doi.org/10.1007/s43452-025-01369-2

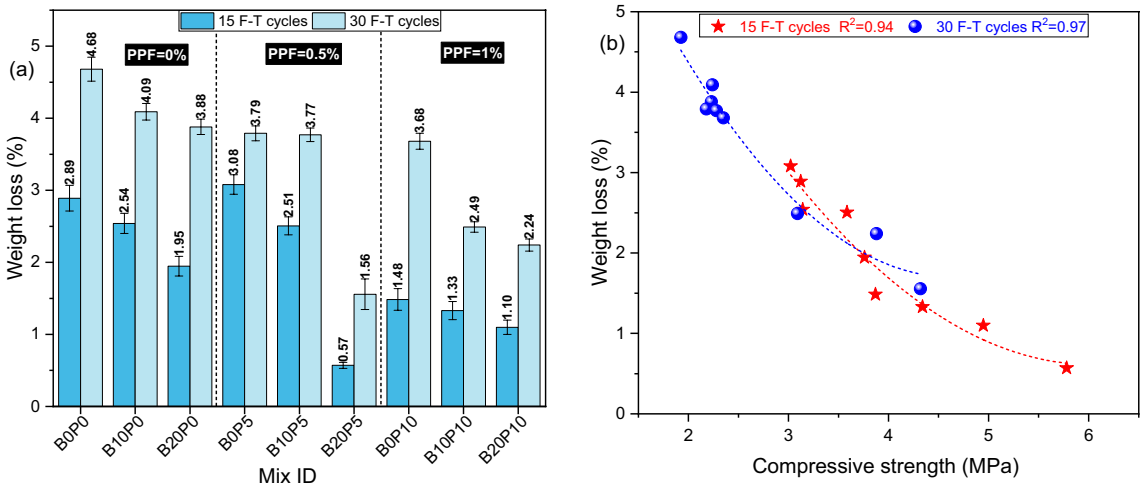

Fig. 17 **a** Following F-T cycles, the weight loss **b** strength versus weight loss

4.2 Weight change after freeze-thaw exposure

Figure 17a shows the impact of replacing FA with BA at substitution levels of 0%, 10%, and 20%, combined with PPF contents of 0%, 0.5%, and 1%, on the average weight loss of GFC mixtures containing 100% PA after exposure to 15 and 30 freeze-thaw (F-T) cycles. The results show that replacing FA with BA and incorporating PPF reduced the weight loss of the mixtures. Among the mixtures, the 0% BA and 0.5% PPF mixture exhibited the largest weight loss after 15 F-T cycles, while the reference mixture (0% BA and 0% PPF) had the largest weight loss after 30 F-T cycles. Conversely, the mixture with 20% BA and 0.5% PPF demonstrated the lowest weight loss after both 15 and 30 F-T cycles. The increased percentage of calcium oxide (CaO) in BA promotes the development of C-S-H gels. By decreasing porosity and increasing the density and cohesiveness of the geopolymer matrix, these gels lessen the material's susceptibility to moisture loss during freeze-thaw cycles. Because the higher BA level resulted in a denser and more cohesive geopolymer matrix, the mixture containing 20% BA lost the least amount of weight. As a result, the material was better able to withstand the strains of expansion and contraction during freeze-thaw cycles and absorbed less water. By serving as crack-bridging agents and preventing cracks from forming and spreading during freeze-thaw cycles, polypropylene fibers aid in weight loss. This reinforcement reduces porosity and strengthens the material's structural integrity [111]. The mixture containing 20% BA and 0.5% PPF lost the least amount of weight because the moderate fiber concentration added just enough reinforcement without creating too many voids. This mixture successfully decreased the material's vulnerability to weight loss brought on by freeze-thaw cycles. A less cohesive matrix resulted from the 0% BA (100% FA) mixture's lack of BA's calcium-based stabilizing properties. In the absence of enough BA, the material's higher porosity resulted in significant weight loss during freeze-thaw cycles and greater water absorption. Although 0.5% PPF offers some reinforcement, the lack of BA resulted in a decrease in the overall integrity of the matrix, which led to the greatest weight loss after 15 F-T cycles. Neither BA's stabilizing effects nor PPF's reinforcement were present in the reference mixture. As a result, the matrix became less cohesive, more porous, and less resistant to freeze-thaw cycles. Following 30 F-T cycles, the material's resistance to weight loss was further weakened by increased water absorption and cumulative micro cracking, which resulted in the greatest weight loss. After 30 cycles, the reference mixture performed poorly as a result of the extended exposure to freeze-thaw stressors, which made its flaws worse. Because the 20% BA and 0.5% PPF mixture coupled the stabilizing impact of BA with the reinforcement of PPF, it performed the best. In order to minimize weight loss during both the 15 and 30 F-T cycles, the moderate PPF content increased crack resistance while the high BA content decreased porosity

and boosted matrix cohesiveness. The denser and more cohesive matrix, combined with fiber reinforcement, allowed the material to better withstand the stresses of freeze-thaw cycles, leading to the lowest weight loss [112].

Figure 17b showed the relationship between compressive strength and weight loss for the mixtures after exposure to 15 and 30 F-T cycles. The trend lines indicated a strong inverse correlation, with R^2 values of 0.94 and 0.97 at 15 and 30 F-T cycles, respectively.

5 Conclusion

This research demonstrates the feasibility of using BA as a partial replacement for FA in GFC, offering a sustainable pathway for waste valorization and enhanced material performance. The incorporation of BA, particularly at a 20% replacement level, significantly improved the mechanical, thermal, and durability properties of GFC. The inclusion of BA and PPF demonstrated significant impacts on the mechanical, thermal, and durability properties of the mixtures. Key findings include:

(a) The mixture containing 20% BA and 0.5% PPF exhibited the highest compressive strength, improving by 41.52% compared to the mixture with 20% BA without PPF.
(b) Flexural strength also reached its peak in the same mixture after 91 days, with the PPF acting effectively as reinforcement by bridging micro-cracks.
(c) Mixtures with 0% PPF and 10% BA showed strength gains at 400 °C and 900 °C. However, the mixture with 20% BA experienced 16.2% strength loss at 400 °C and 27.1% at 900 °C, highlighting the destabilizing effect of excessive BA and PPF content at high temperatures.
(d) At elevated temperatures, PPF degradation created voids, and high BA content contributed to shrinkage and micro-cracking, reducing thermal stability.
(e) After 15 freeze-thaw cycles, the mixture with 0% BA (100% FA) and 1% PPF exhibited the largest strength gain (50.58%), while the mixture with 20% BA and 0.5% PPF demonstrated the lowest weight loss, emphasizing its resilience to freeze-thaw effects.
(f) Strength losses were observed after 30 freeze-thaw cycles, with the mixture containing 20% BA and 0% PPF showing the largest loss (32.01%).
(g) The porosity and water absorption rates were lowest in the mixture containing 20% BA and 0.5% PPF, reducing water absorption by over 40% compared to the reference mixture (100% FA and 0% PPF).
(h) Sorptivity also showed a strong inverse relationship with compressive strength, with the most optimized mixture achieving the lowest sorptivity value (8.28%).
(i) The highest dry unit weight (1788 kg/m³) and thermal conductivity (0.619 W/mK) were recorded in the mixture with 20% BA and 0.5% PPF, reflecting enhanced matrix densification.
(j) A strong correlation ($R^2 = 0.97$) was observed between dry unit weight and thermal conductivity.
(k) Replacing FA with BA up to 20% aligns with sustainable construction practices by utilizing industrial by-products, reducing dependency on traditional binders, and enhancing material properties.
(l) SEM analysis revealed that BA's angular particles improved particle packing and promoted the formation of dense binding gels, while PPF effectively bridged micro cracks and minimized pore connectivity, further enhancing the mechanical and durability properties.

The results underscore the potential of combining BA and PPF to produce GFC with tailored mechanical, thermal, and durability properties. Future work should explore the effects of alternative curing regimes and extended exposure to extreme environmental conditions to further optimize the material for sustainable construction applications.

Funding This research received no external funding.

Data availability The data that support the findings of this study are available from the corresponding author upon reasonable

request.

Declarations

Conflict of interest The author declares that he has no conflict of interest.

Ethical approval This article does not contain any studies with human participants or animals performed by any of the authors.

References

1. Tran NP, Nguyen TN, Ngo TD, Le PK, Le TA. Strategic progress in foam stabilisation towards high-performance foam concrete for building sustainability: a state-of-the-art review. J Clean Prod. 2022;375:133939.1-27
2. Wagh CD, Gandhi ISR. Investigations on the performance of Xanthan gum as a foam stabilizer and assessment of economic and environmental impacts of foam concrete production. J Building Eng. 2024;82:108286.1-23
3. Bayraktar OY, Özel HB, Benli A, Yılmazoğlu MU, Türkel İ, Dal BB, Şevik H, Kaplan G. Sustainable foam concrete development: enhancing durability and performance through pine cone powder and fly Ash incorporation in alkali-activated geopolymers. Constr Build Mater. 2024;457:139422.1-23
4. Benli A. Sustainable use of waste glass sand and waste glass powder in alkali-activated slag foam concretes: physico-mechanical, thermal insulation and durability characteristics. Constr Build Mater. 2024;38:137128.1-20
5. Özkan IGM, Aldemir K, Alhasan O, Benli A, Bayraktar OY, Yilmazoglu MU, Kaplan G. Investigation on the sustainable use of different sizes of sawdust aggregates in eco-friendly foam concretes: Physico-mechanical, thermal insulation and durability characteristics. Constr Build Mater. 2024;438:137100.
6. Bayraktar OY, Yarar G, Benli A, Kaplan G, Gencel O, Sutcu M, Kozlowski M, Kadela M. Basalt fiber reinforced foam concrete with marble waste and calcium aluminate cement. Struct Concrete. 2023;24(1):1152–78.
7. Bayraktar OY, Kaplan G, Gencel O, Benli A, Sutcu M. Physico-mechanical, durability and thermal properties of basalt fiber reinforced foamed concrete containing waste marble powder and slag. Constr Build Mater. 2021;288:123128.
8. Reddy KC, Vinod B. Characterization and Preparation of eco-friendly foamed concrete using a foaming agent: optimizing the design by Taguchi analysis. J Building Eng. 2024;88:109068.
9. Maglad AM, Mydin MAO, Majeed SS, Tayeh BA, Tobbala DE. Exploring the influence of calcinated eggshell powder on lightweight foamed concrete: a comprehensive study on freshness, mechanical strength, thermal characteristics and transport properties. J Building Eng. 2024;87:108966.
10. Alharthai M, Mydin MAO, Majeed SS, Tayeh BA, Tobbala DE. Synthesis and characterisation of ZnO nanoparticles and its influence on the engineering properties of lightweight foamed concrete. Arch Civ Mech Eng. 2025;25(2):79.
11. Bodur B, Benli A, Bayraktar OY, Alcan HG, Kaplan G, Aydin AC. Impact of attapulgite and basalt fiber additions on the performance of pumice-based foam concrete: mechanical, thermal, and durability properties. Arch Civ Mech Eng. 2025;25(2).
12. Gencel O, Ustaoglu A, Benli A, Hekimoglu G, Sari A, Erdogmus E, Sutcu M, Kaplan G, Bayraktar OY. Investigation of physico-mechanical, thermal properties and solar thermoregulation performance of shape-stable attapulgite based composite phase change material in foam concrete. Sol Energy. 2022;236:51–62.
13. Gencel O, Benli A, Bayraktar OY, Kaplan G, Sutcu M, Elabade WAT. Effect of waste marble powder and rice husk Ash on the microstructural, physico-mechanical and transport properties of foam concretes exposed to high temperatures and freeze-thaw cycles. Constr Build Mater. 2021;291.
14. Gencel O, Bayraktar OY, Kaplan G, Benli A, Martinez-Barrera G, Brostow W, Tek M, Bodur B. Characteristics of hemp fibre reinforced foam concretes with fly Ash and Taguchi optimization. Constr Build Mater. 2021;294:123607.
15. Dener M, Altunhan U, Benli A. A green binder for cold weather applications: enhancing mechanical performance of alkali-activated slag through modulus, alkali dosage, and Portland cement substitution. Arch Civ Mech Eng. 2024;24(3):176.
16. Turkoglu M, Bayraktar OY, Benli A, Kaplan G. Effect of cement clinker type, curing regime and activator dosage on the performance of one-part alkali-activated hybrid slag/clinker composites. J Building Eng. 2023;68:106604.
17. Zhu XH, Luan MY, Tang DS, Yang K, Yang CH. Understanding the setting behaviours of alkali-activated slag from the dissolution-precipitation point of view. Cem Concrete Comp. 2024;148.
18. Bayraktar OY, Benli A, Bodur B, Öz A, Kaplan G. Performance assessment and cost analysis of slag/metakaolin based rubberized semi-lightweight geopolymers with perlite aggregate: sustainable reuse of waste tires. Constr Build Mater. 2024;411.
19. Ahiskali A, Benli A, Ahiskali M, Bayraktar OY, Kaplan G. Sustainable geopolymer foam concrete with recycled crumb rubber and dual fiber reinforcement of polypropylene and glass fibers: A comprehensive study. Constr Build Mater. 2025;474.

20. Abellan-Garcia J, Redondo-Mosquera J, Khan MI, Abbas YM, Castro-Cabeza A. Development of a novel 124 MPa strength green reactive powder concrete employing waste glass and locally available cement. Arch Civ Mech Eng. 2023;23(3).
21. Bodur B, Bayraktar OY, Benli A, Kaplan G, Tobbala DE, Tayeh B. Effect of using wastewater from the ready-mixed concrete plant on the performance of one-part alkali-activated GBFS/FA composites: Fresh, mechanical and durability properties. J Building Eng. 2023;76.
22. Bayrak B, Benli A, Alcan HG, Çelebi O, Kaplan G, Aydin AC. Recycling of waste marble powder and waste colemanite in ternary-blended green geopolymer composites: Mechanical, durability and microstructural properties. J Building Eng. 2023;73.
23. Ranjbar N, Kuenzel C, Spangenberg J, Mehrali M. Hardening evolution of geopolymers from setting to equilibrium: A review. Cem Concrete Comp. 2020;114.
24. Nematollahi B, Ranade R, Sanjayan J, Ramakrishnan S. Thermal and mechanical properties of sustainable lightweight strain hardening geopolymer composites. Arch Civ Mech Eng. 2017;17(1):55–64.
25. Sate V, Sathonsaowaphak A, Chindaprasirt P. Resistance of lignite bottom Ash geopolymer mortar to sulfate and sulfuric acid attack. Cem Concrete Comp. 2012;34(5):700–8.
26. Bayraktar OY, Bozkurt TH, Benli A, Koksal F, Tuerkoglu M, Kaplan G. Sustainable one-part alkali activated slag/fly Ash Geo-SIFCOM containing recycled sands: Mechanical, flexural, durability and microstructural properties. Sustain Chem Pharm. 2023;36.
27. Yang KH, Lee KH, Song JK, Gong MH. Properties and sustainability of alkali-activated slag foamed concrete. J Clean Prod. 2014;68:226–33.
28. Abd Elrahman M, Sikora P, Chung SY, Stephan D. The performance of ultra-lightweight foamed concrete incorporating Nanosilica. Arch Civ Mech Eng. 2021;21(2).
29. Dhasindrakrishna K, Pasupathy K, Ramakrishnan S, Sanjayan J. Progress, current thinking and challenges in geopolymer foam concrete technology. Cem Concrete Comp. 2021;116.
30. Thomas BS, Yang J, Mo KH, Abdalla JA, Hawileh RA, Ariyachandra E. Biomass ashes from agricultural wastes as supplementary cementitious materials or aggregate replacement in cement/geopolymer concrete: A comprehensive review. J Building Eng. 2021;40.
31. Tu WL, Fang GH, Dong BQ, Zhang MZ. Micromechanical analysis of alkali-activated fly ash-slag paste subjected to elevated temperatures. Cem Concrete Comp. 2024;53.
32. Kovtun M, Ziolkowski V, Shekhovtsova J, Kearsley E. Direct electric curing of alkali-activated fly Ash concretes: a tool for wider utilization of fly Ashes. J Clean Prod. 2016;133:220–7.
33. Althoey F, Zaid O, Alsharari F, Yosri AM, Isleem HF. Evaluating the impact of nano-silica on characteristics of self-compacting geopolymer concrete with waste tire steel fiber. Arch Civ Mech Eng. 2025;25(2).
34. Fernando S, Gunasekara C, Law DW, Nasvi MCM, Setunge S, Dissanayake R, Ismail MGMU. Investigation of the reaction mechanism of blended fly Ash and rice husk Ash alkali-activated binders. Arch Civ Mech Eng. 2021;22(1).
35. Arslan S, Öz A, Benli A, Bayrak B, Kaplan G, Aydin AC. Sustainable use of silica fume and Metakaolin in slag/fly ash-based self-compacting geopolymer composites: Fresh, physico-mechanical and durability properties. Sustain Chem Pharm. 2024;38.
36. Su LJ, Fu GS, Liang B, Sun Q, Zhang XD. Mechanical properties and microstructure evaluation of fly ash-Slag geopolymer foaming materials. Ceram Int. 2022;48(13):18224–37.
37. Das P, Cheela VRS, Mistri A, Chakraborty S, Dubey B, Barai SV. Performance assessment and life cycle analysis of concrete containing ferrochrome slag and fly Ash as replacement materials–a circular approach. Constr Build Mater. 2022;347:128609.
38. Das P, Chakraborty S, Barai SV. Flexural behaviour of fly Ash incorporated ferrochrome slag aggregate reinforced concrete beam. J Building Eng. 2023;76:107317.
39. Yassen MM, Hama SM, Mahmoud AS. Shear behavior of reinforced concrete beams incorporating waste glass powder as partial replacement of cement. Eur J Environ Civil Eng. 2023;27(5):2194–209.
40. Soe PS, Sornlar W, Wannagon A, Chaysuwan D. Mechanical and thermal properties of bottom ash-based porous geopolymer as thermal insulation material for construction. J Mater Cycles Waste Manage. 2023;25(5):2964–75.
41. Hosseini S, Brake NA, Nikookar M, Günaydin-Sen Ö, Snyder HA. Mechanochemically activated bottom Ash-fly Ash geopolymer. Cem Concrete Comp. 2021;118.
42. Suksiripattanapong C, Krosoongnern K, Thumrongvut J, Sukontasukkul P, Horpibulsuk S, Chindaprasirt P. Properties of cellular lightweight high calcium bottom ash-portland cement geopolymer mortar. Case Stud Constr Mater. 2020;12.
43. Kim H, Lee J-Y. Effect of ash particle sizes on the compressive strength and thermal conductivity of geopolymer synthesized with alkali activated low-calcium ground coal bottom ash, 2017 World of Coal Ash (WOCA) Conference in Lexington, KY, May 9–11, 2017.
44. Kalaw ME, Kalaw JM, Promentilla MA. Geopolymers synthesized from Philippine coal Ash as sustainable alternative low heat transmission and fire-resistant material for buildings. ASEAN Eng J. 2021;11(3):45–56.

45. Althoey F, Zaid O, Alsulamy S, Martínez-García R, de Prado-Gil J, Arbili MM. Experimental study on the properties of ultra-high-strength geopolymer concrete with polypropylene fibers and nano-silica. PLoS ONE. 2023;18(4).
46. Tayeh BA, Akeed MH, Qaidi S, Abu Bakar BH. Influence of Microsilica and polypropylene fibers on the fresh and mechanical properties of ultra-high performance geopolymer concrete (UHP-GPC). Case Stud Constr Mater. 2022;17.
47. Zeyad AM, Magbool HM, Mutnbak M, Amin M, Agwa IS. Effect of steel fibers, polypropylene fibers, and silica fume on the properties of ultra-high-performance geopolymer concrete. Arch Civ Mech Eng. 2025;25(4).
48. Liu T, Zhao G, Qu B, Gong C. Characterization of a fly ash-based hybrid well cement under different temperature curing conditions for natural gas hydrate drilling. Constr Build Mater. 2024;445:137874.
49. Kong DLY, Sanjayan JG. Effect of elevated temperatures on geopolymer paste, mortar and concrete. Cem Concr Res. 2010;40(2):334–9.
50. ASTM. ASTM C1437–15 standard test method for flow of hydraulic cement mortar. West Conshohocken, PA: ASTM International; 2015.
51. ASTM C642–13 Standard Test Method for Density, Absorption, and Voids in Hardened Concrete. West Conshohocken, PA: ASTM International. 2013.
52. ASTM. ASTM C348–19 standard test method for flexural strength of Hydraulic-Cement mortars. West Conshohocken, PA.: ASTM International; 2019.
53. ASTM. ASTM C349–18 Standard Test Method for Compressive Strength of Hydraulic-Cement Mortars (Using Portions of Prisms Broken in Flexure).ASTM International, West Conshohocken, PA., 2018.
54. EN 1015-18. Methods of test for mortar for Masonry – Part 18: determination of water absorption coefficient due to capillary action of hardened mortar. Brussels, Belgium: European Committee for Standardization (CEN); 2002.
55. ASTM C666/C666M-15. 2015 standard test method for resistance of concrete to rapid freezing and thawing. ASTM International, West Conshohocken, PA.
56. ASTM C596-. 23 Standard Test Method for Drying Shrinkage of Mortar Containing Hydraulic Cement.
57. Sun YB, Liu ZY, Ghorbani S, Ye G, De Schutter G. Fresh and hardened properties of alkali-activated slag concrete: the effect of fly Ash as a supplementary precursor. J Clean Prod. 2022;370
58. Yang T, Zhu HJ, Zhang ZH, Gao X, Zhang CS, Wu QS. Effect of fly Ash microsphere on the rheology and microstructure of alkali-activated fly Ash/slag pastes. Cem Concr Res. 2018;109:198–207.
59. Gómez-Casero MA, Sánchez-Soto PJ, Castro E, Eliche-Quesada D. Effect of olive-pruning fibres as reinforcements of alkali-activated cements based on electric Arc furnace slag and biomass bottom Ash. Arch Civ Mech Eng. 2024;24(2).
60. Si RZ, Guo SC, Dai QL. Influence of calcium content on the atomic structure and phase formation of alkali-activated cement binder. J Am Ceram Soc. 2019;102(3):1479–94.
61. Puligilla S, Mondal P. Role of slag in microstructural development and hardening of fly ash-slag geopolymer. Cem Concr Res. 2013;43:70–80.
62. Patrisia Y, Law D, Gunasekara C, Wardhono A. The role of Na2O dosage in iron-rich fly Ash geopolymer mortar. Arch Civ Mech Eng. 2022;22(4).
63. Hossain FMZ, Shahjalal M, Islam K, Tiznobaik M, Alam MS. Mechanical properties of recycled aggregate concrete containing crumb rubber and polypropylene fiber. Constr Build Mater. 2019;225:983–96.
64. Ranjbar N, Talebian S, Mehrali M, Kuenzel C, Metselaar HSC, Jumaat MZ. Mechanisms of interfacial bond in steel and polypropylene fiber reinforced geopolymer composites. Compos Sci Technol. 2016;122:73–81.
65. Shi YX, Zhang ZY, Sang ZH, Zhao QX. Microstructure and composition of red Mud-Fly Ash-Based geopolymers incorporating carbide slag. Front Mater. 2020;7 .
66. Niklioc I, Markovic S, Jankovic-Castvan I, Radmilovic VV, Karanovic L, Babic B, Radmilovic VR. Modification of mechanical and thermal properties of fly ash-based geopolymer by the incorporation of steel slag. Mater Lett. 2016;176:301–5.
67. Nuaklong P, Wongsa A, Sata V, Boonserm K, Sanjayan J, Chindaprasirt P. Properties of high-calcium and low-calcium fly Ash combination geopolymer mortar containing recycled aggregate. Heliyon. 2019;5(9).
68. Saini G, Vattipalli U. Assessing properties of alkali activated GGBS based self-compacting geopolymer concrete using nano-silica. Case Stud Constr Mater. 2020;12.
69. Islam A, Alengaram UJ, Jumaat MZ, Bashar II. The development of compressive strength of ground granulated blast furnace slag-palm oil fuel Ash-fly Ash based geopolymer mortar. Mater Design. 2014;56:833–41.
70. Ranjbar N, Mehrali M, Mehrali M, Alengaram UJ, Jumaat MZ. Graphene nanoplatelet-fly Ash based geopolymer composites. Cem Concr Res. 2015;76:222–31.
71. Bodur B, Isik MAM, Benli A, Bayrak B, Öz A, Bayraktar OY, Kaplan G, Aydin AC. Durability of green rubberized 3D printed lightweight cement composites reinforced with micro attapulgite and micro steel fibers: printability and environmental perspective. J Building Eng. 2024;90.
72. Zhang Z-h, Yao X, Zhu H-j, Hua S-d, Chen Y. Preparation and mechanical properties of polypropylene fiber reinforced calcined kaolin-fly Ash based geopolymer. J Cent South Univ T. 2009;16(1):49–52.
73. Chindaprasirt P, Boonbamrung T, Poolsong A, Kroehong W. Effect of elevated temperature on polypropylene fiber reinforced alkali-activated high calcium fly Ash paste. Case Stud Constr Mater. 2021;15.

74. Baykara H, Cornejo MH, Espinoza A, Garcia E, Ulloa N. Preparation, characterization, and evaluation of compressive strength of polypropylene fiber reinforced geopolymer mortars. Heliyon. 2020;6(4).
75. Sukontasukkul P, Pongsopha P, Chindaprasirt P, Songpiriyakij S. Flexural performance and toughness of hybrid steel and polypropylene fibre reinforced geopolymer. Constr Build Mater. 2018;161:37–44.
76. Al-Mashhadani MM, Canpolat O, Aygormez Y, Uysal M, Erdem S. Mechanical and microstructural characterization of fiber reinforced fly Ash based geopolymer composites. Constr Build Mater. 2018;167:505–13.
77. Wang XD, Cheng CX, Wang XZ, Sun MG. Study on the mechanical properties of rice husk ash-based geopolymer-regenerated mortar reinforced by polyimide fiber and carbon fiber after high-temperature exposure. Arch Civ Mech Eng. 2025;25(3).
78. Guo XL, Shi HS, Lin MS, Dong WJ. Effects of calcium contents in class C fly Ash geopolymer. Progress Polym Concrete. 2013;687:508–13.
79. van Deventer JSJ, Provis JL, Duxson P. Technical and commercial progress in the adoption of geopolymer cement. Min Eng. 2012;29:89–104.
80. Li YH, Chen P, Chen ZX, Liu XH, Liu ZM, Liu YB. Influence of fiber on the shrinkage performance of alkali-activated slag recycled concrete. Arch Civ Mech Eng. 2024;24(3).
81. Kilic AT, Uysal M, Aygun BF, Nazir K, Canpolat O, Dilbas H. Multi-criteria decision-making optimization-based fiber-reinforced waste ceramic powder-based geopolymer: toward a sustainable net zero/low CO2 emission Building material. Arch Civ Mech Eng. 2024;24(4):242.
82. Chu H, Qin J, Gao L, Jiang J, Wang F, Wang L. A cost-effective approach to manufacturing ultra-high-performance lightweight concrete via air-entraining. Arch Civ Mech Eng. 2023;23(3):210.
83. Raj A, Sathyan D, Mini KM. Physical and functional characteristics of foam concrete: A review. Constr Build Mater. 2019;221:787–99.
84. Bayraktar OY, Tunçtan M, Benli A, Türkel I, Kizilay G, Kaplan G. A study on sustainable foam concrete with waste polyester and ceramic powder: properties and durability. J Building Eng. 2025;95.
85. Huang Z, Luo Y, Zhang W, Ye Z, Li Z, Liang Y. Thermal insulation and high-temperature resistant cement-based materials with different pore structure characteristics: performance and high-temperature testing. J Building Eng. 2025;111839:1-24.
86. Akbar A, Farooq F, Shafique M, Aslam F, Alyousef R, Alabduljabbar H. Sugarcane Bagasse ash-based engineered geopolymer mortar incorporating propylene fibers. J Building Eng. 2021;33.
87. Huseien GF, Shah KW. Durability and life cycle evaluation of self-compacting concrete containing fly Ash as GBFS replacement with alkali activation. Constr Build Mater. 2020;235.
88. Aragoncillo AM, Cleary D, Thayasivam U, Lomboy G. Water sorptivity prediction model for concrete with all coarse recycled concrete aggregates. Constr Build Mater. 2023;394:132128.
89. Paktiawal A, Alam M. Experimental evaluation of sorptivity for high strength concrete reinforced with zirconia rich glass fiber and basalt fiber. Mater Today Proc. 2021.
90. Benli A, Karatas M, Bakir Y. An experimental study of different curing regimes on the mechanical properties and sorptivity of self-compacting mortars with fly Ash and silica fume. Constr Build Mater. 2017;144:552–62.
91. Kaplan G, Coskan U, Benli A, Bayraktar OY, Kucukbaltaci AB. The impact of natural and calcined zeolites on the mechanical and durability characteristics of glass fiber reinforced cement composites. Constr Build Mater. 2021;311.
92. Cantero B, del Bosque IFS, Matias A, de Rojas MIS, Medina C. Water transport mechanisms in concretes bearing mixed recycled aggregates. Cem Concrete Comp. 2020);107
93. Deng ZM, Deng ZJ. Short-term improvement of ductile geopolymer composites exposed to magnesium sulfate: mechanical properties, sorptivity, and mechanisms. Constr Build Mater. 2023;408.
94. Gencel O, Bayraktar OY, Kaplan G, Arslan O, Nodehi M, Benli A, Gholampour A, Ozbakkaloglu T. Lightweight foam concrete containing expanded perlite and glass sand: Physico-mechanical, durability, and insulation properties. Constr Build Mater. 2022;320.
95. Gencel O, Nodehi M, Bayraktar OY, Kaplan G, Benli A, Gholampour A, Ozbakkaloglu T. Basalt fiber-reinforced foam concrete containing silica fume: an experimental study. Constr Build Mater. 2022;326.
96. Huang Y. Influence of calcium bentonite addition on the compressive Strength, efflorescence extent and drying shrinkage of Fly-Ash based geopolymer mortar. T Indian Ceram Soc. 2020;79(2):77–82.
97. Bouziadi F, Boulekbache B, Hamrat M. The effects of fibres on the shrinkage of high-strength concrete under various curing temperatures. Constr Build Mater. 2016;114:40–8.
98. Zhu Jf, Wang Zq, Tao Yl, Ju Ly, Yang H. Macro–micro investigation on stabilization sludge as subgrade filler by the ternary blending of steel slag and fly Ash and calcium carbide residue. J Clean Prod. 2024;447:141496.
99. Mahdi SN, Babu RDV, Hossiney N, Abdullah MMA. Strength and durability properties of geopolymer paver blocks made with fly Ash and brick kiln rice husk Ash. Case Stud Constr Mater. 2022;16.
100. Shihada S. Effect of polypropylene fibers on concrete fire resistance. J Civil Eng Manage. 2011;17(2):259–64.
101. Hager I, Sitarz M, Mroz K. Fly-ash based geopolymer mortar for high-temperature application - Effect of slag addition. J Clean Prod. 2021;316.

102. Yilmazoglu MU, Kara HO, Benli A, Demirkiran AR, Bayraktar OY, Kaplan G. Sustainable alkali-activated foam concrete with pumice aggregate: effects of clinoptilolite zeolite and fly Ash on strength, durability, and thermal performance. Constr Build Mater. 2025;464.
103. Bayrak B, Öz A, Benli A, Kavaz E, Kaplan G, Aydin AC. Physico-mechanical and shielding properties of alkali-activated slag composites incorporating cement clinker aggregate: effect of high temperature and particle size. J Building Eng. 2023;67.
104. Koksal F, Nazli T, Benli A, Gencel O, Kaplan G. The effects of cement type and expanded vermiculite powder on the thermo- mechanical characteristics and durability of lightweight mortars at high temperature and RSM modelling. Case Stud Constr Mater. 2021;15.
105. Koksal F, Kocabeyoglu ET, Gencel O, Benli A. The effects of high temperature and cooling regimes on the mechanical and durability properties of basalt fiber reinforced mortars with silica fume. Cem Concrete Comp. 2021;121:104107.
106. Karatas M, Benli A, Arslan F. The effects of Kaolin and calcined Kaolin on the durability and mechanical properties of self-compacting mortars subjected to high temperatures. Constr Build Mater. 2020;265:120300.
107. Kaya M, Bayram M, Hossein S, Xiao J, Gencel O, Ozbakkaloglu T. Physico-mechanical properties of dolomite-based geopolymers produced with zeolite aggregates. Arch Civ Mech Eng. 2025;25(4):181.
108. Öz A, Yilmaz MK, Benli A, Kaplan G. Sustainable prepacked alkali-activated concrete: influence of natural zeolite, recycled aggregate, and curing conditions on mechanical, durability, and thermal performance. Arch Civ Mech Eng. 2025;25:5–6.
109. Yuan Y, Zhao RD, Li R, Wang YB, Cheng ZQ, Li FH, Ma ZGJ. Frost resistance of fiber-reinforced blended slag and class F fly ash-based geopolymer concrete under the coupling effect of freeze-thaw cycling and axial compressive loading. Constr Build Mater. 2020;250:118831.
110. Alsaif A, Albidah A, Abadel A, Abbas H, Al-Salloum Y. Development of metakaolin-based geopolymer rubberized concrete: fresh and hardened properties. Arch Civ Mech Eng. 2022;22(3).
111. Xu Y, Ye H, Yuan Q, Shi C, Gao Y, Fu QJAoC. The durability of concrete subject to mechanical load coupled with freeze–thaw cycles: A review. Arch Civ Mech Eng. 2022;22(1):47.
112. Demir B, Bayraktar OY, Benli A, Türkel İ, Kara HO, Kaplan G. Recycling concrete sludge waste as a supplementary binder in one-part alkali-activated composites: A comprehensive performance evaluation. Sustain Chem Pharm. 2025;48:102245.

Authors and Affiliations

İhsan Türkel[1] · Mehmet Uğur Yılmazoğlu[1] · Mehmet Akif Alman[1] · Ahmet Benli[2] · Oğuzhan Yavuz Bayraktar[1] · Gökhan Kaplan[3]

✉ Ahmet Benli
ahbenli@hotmail.com

[1] Faculty of Engineering and Architecture, Civil Engineering Department, Kastamonu University, Kastamonu 37150, Türkiye

[2] Faculty of Engineering and Architecture, Civil Engineering Department, Bingol University, Bingol 12100, Türkiye

[3] Faculty of Engineering, Civil Engineering Department, Atatürk University, Erzurum 25030, Türkiye